

Multi-Agent Collaborative Intelligence: Dual-Dial Control for Reliable LLM Reasoning

Edward Y. Chang, Ethan Y. Chang
Stanford University, UIUC

Abstract

Multi-agent debate often wastes compute by using a fixed adversarial stance, aggregating without deliberation, or stopping on heuristics. We introduce MACI, an active controller with two independent dials that decouple information from behavior: an information dial that gates evidence by quality, and a behavior dial that schedules contentiousness from exploration to consolidation. A moderator tracks disagreement, overlap, evidence quality, and argument quality, and halts when gains plateau. We provide theory-lite guarantees for nonincreasing dispersion and provable termination, with a budget-feasible scheduler. Across clinical diagnosis and news-bias tasks, MACI improves accuracy and calibration while reducing tokens, and converts residual uncertainty into precision RAG plans that specify what to retrieve next. We use a cross-family LLM judge (CRIT) as a conservative soft weight and stop signal, validated for order invariance and judge-swap stability; stability depends on using high-capability judges. MACI turns debate into a budget-aware, measurable, and provably terminating controller.

1 Introduction

Despite intense interest, multi-agent debate has seen limited progress in theory or practice. Unmoderated or ad hoc collaboration lacks provable termination, calibrated uncertainty, and cost control [Cemri et al., 2025]. Common approaches use a fixed adversarial stance [Liang et al., 2024], aggregate without deliberation [Wang et al., 2023], or stop on heuristics, which wastes compute and locks in early errors.

The control problem. Reliable multi-agent reasoning requires *active modulation*. Early rounds should

explore alternatives, and later rounds should consolidate on well-supported conclusions. This demands two independent controls—what information enters (evidence gating) and how agents interact (behavioral stance)—together with principled stopping that detects convergence.

Beyond single-dial modulation. Prior work introduced contentiousness modulation [Chang, 2023a,b], showing that behavior matters, but a single dial is insufficient. Systems need concurrent control over information quality and interaction intensity, and they must stop when additional debate yields diminishing returns. The CRIT framework [Chang, 2023a] evaluates arguments but has not been coupled to systematic stopping.

MACI: Dual dials with measured stopping. We present MACI (Multi-Agent Collaborative Intelligence), an active controller with two orthogonal dials. The *information* dial (τ) gates evidence by quality, and the *behavior* dial (CL) schedules contentiousness from exploration to consolidation. A moderator tracks four signals—disagreement (D_{JS}), overlap (O)¹, evidence quality (Q), and argument quality (CRIT)—and halts when gains plateau. Beyond prediction, MACI translates residual uncertainty into precision RAG: targeted acquisition plans that specify what to retrieve next.

Guarantees and scheduler. Under gated averaging with smoothing, dispersion is nonincreasing and the plateau test terminates in $O(1/\varepsilon)$ rounds, improving to $O(\log(1/\varepsilon))$ under a contraction condition (Lem. 1, Prop. 2, Appx. M). A budget-feasible UCB scheduler over $(\Delta\alpha, \Delta\gamma)$ achieves $\tilde{O}(\sqrt{KT})$ no-regret with zero expected budget violation (Prop. 1, Appx. L).

Empirical highlights. On clinical diagnosis with 1,500 cases spanning 100+ diseases, MACI improves Acc@1 by **+3.9 pp** over majority vote and **+3.7 pp**

¹Overlap is not synonymous with agreement; it measures convergence of *evidence*, whereas disagreement measures convergence of *beliefs*. We require both.

Table 1: Multi-agent orchestration methods: architectural comparison.

Method	Info	Gate	Behavior	Ctrl	Stopping	Signals	Notes
<i>Aggregation methods</i>							
Majority Vote Choi et al. [2025a]		✗	✗		Fixed (N)	–	Passive aggregation
Self-Consistency Wang et al. [2023]		✗	✗		Fixed (N)	–	Fixed sampling
Mixture-of-Agents Wang et al. [2024b]		✗	✗		Heuristic	–	Layered ensemble
<i>Fixed-stance debate</i>							
Liang et al. Liang et al. [2024]		✗		Fixed	Heuristic	–	Fixed adversarial roles
Diverse MAD Liu et al. [2025]		✗		Varied	Heuristic	–	Prompting style variation
Multi-LLM Debate Estornell and Liu [2024]		✗		Fixed	Heuristic	–	Ad hoc termination
<i>Adaptive orchestration</i>							
MACI (ours)		✓		Scheduled	Plateau	4	Dual-dial control

over fixed-contentiousness debate, reduces calibration error (ECE **0.081** vs. 0.103), and uses **19% fewer** generation tokens. A cross-domain study on news bias (619 articles) shows portability: the same controls narrow the partisan gap by **68%** without domain tuning. MACI also translates residual uncertainty into *precision RAG* plans that specify what to retrieve next to improve decision quality.

Contributions. We operationalize these ideas into five contributions:

1. *Dual control.* Two-dial orchestration with information-theoretic stopping, where $D(t)$ is nonincreasing and plateau tests terminate within bounded rounds (Lem. 1, Prop. 2).
2. *Judge robustness.* CRIT is order invariant and stable under cross-family judge swaps (Appx. E.7; $n=100$, 2–3% winner flips; $\alpha=0.68$); we use it as a soft weight and part of a compound stop rule, not a hard oracle.
3. *Targeted acquisition.* Systematic collaboration yields predictions together with precision RAG plans for underspecified problems.
4. *Empirical validation.* Improvements in accuracy, calibration, and efficiency across two domains, with complete ablations and transcripts.

Evaluator reliability. We rely on CRIT, a cross-family judge that scores evidence-, logic-, and relevance-grounded argument quality. We validate order invariance and judge-swap stability ($n=100$; 2–3% winner flips) and report tentatively acceptable agreement (Krippendorff’s $\alpha=0.68$). We therefore use CRIT as a soft aggregation weight and as part of a compound stop rule, rather than as a hard oracle. Stability holds with high-capability judges; weaker or poorly aligned judges may require larger K , tighter thresholds, or periodic human audits (Appx. E.7).

2 Related Work

Multi-agent debate and orchestration. Debate-style prompting aims to surface errors through agent

opposition [Irving et al., 2018], yet implementations often collapse to majority opinions or underperform strong single models [Wang et al., 2024b, Smit et al., 2024, Estornell and Liu, 2024, Choi et al., 2025b]. For example, Liang et al. [Liang et al., 2024] maintain fixed adversarial intensity throughout, wasting tokens when contention becomes unproductive. Diverse Multi-Agent Debate [Liu et al., 2025] varies agent prompting styles but lacks behavioral adaptation within debates. Recent audits reveal that multi-agent systems frequently fail without systematic orchestration [Cemri et al., 2025], motivating principled control mechanisms.

Table 1 reveals a critical gap: existing methods provide either no control or single-axis control (fixed/varied debate intensity), but none combine independent information gating with scheduled behavioral transitions. *Aggregation methods* sample diverse responses but aggregate without deliberation, causing performance degradation as answer spaces grow [Choi et al., 2025b]. *Fixed-stance debate* methods maintain constant intensity, unable to transition from exploratory disagreement to consolidative synthesis. MACI addresses both limitations: an information dial filters evidence by quality while a behavior dial schedules contentiousness from high to low, with information-theoretic stopping that detects convergence plateaus rather than relying on heuristic round limits. **To our knowledge, no prior work provides independent controls over information quality and behavioral stance.**

Computational paradigms and capability trade-offs. Transformers [Vaswani et al., 2017] required orders of magnitude more computation than RNNs but unlocked scaling laws [Kaplan et al., 2020]; large language models [Brown et al., 2020] continue this trend. MACI follows this paradigm: systematic orchestration requires overhead, but provides measurable gains in accuracy, calibration, and epistemic humility. For high-stakes applications, reliability justifies cost.

Ensemble methods and aggregation. Self-Consistency [Wang et al., 2023] and majority voting aggregate sampled chains with fixed behavior. Mixture-

of Agents [Wang et al., 2024a, Li et al., 2025] improves performance via layered ensembles but under-specifies convergence beyond heuristic rounds. These methods assume weak error correlation and rarely specify stopping criteria. On short-horizon multiple-choice tasks, voting can dominate when answer spaces are small [Choi et al., 2025b], but performance degrades as dimensionality grows (Appendix K). MACI differs by using information-theoretic signals (disagreement, overlap, evidence quality) to drive active deliberation with plateau-based stopping.

Control and stopping in AI systems. Control-theoretic approaches in reinforcement learning use measured feedback to adjust policy parameters [Recht, 2019]. Active learning frameworks gate information acquisition based on uncertainty [Settles, 2009]. Our work extends these ideas to multi-agent reasoning: the moderator tracks four signals and adjusts behavioral stance when progress plateaus, analogous to adaptive control in dynamical systems. Prior debate work lacks this closed-loop structure, relying instead on fixed interaction patterns or ad hoc stopping rules.

Initialization and few-shot learning. Bayesian [Xie et al., 2022], meta-learning [Dai et al., 2023], and optimization-as-inference [von Oswald et al., 2023] perspectives explain in-context learning. Selection and weighting strategies adapt which demonstrations matter [Hong et al., 2025, Wang et al., 2024c]. We use lightweight information-theoretic metrics (pattern density, prior-target mismatch) to initialize debate parameters. Appendix F validates these heuristics on controlled tasks; broader ICL theory appears in concurrent work.

Evaluation with LLM judges. Independent LLM judges are appealing, but evaluators can exhibit self-preference bias, especially when sharing a family with the debaters [Panickssery et al., 2024]. Moreover, recent scalable-oversight studies report that weak-judge regimes yield inconsistent gains [Kenton et al., 2024]. *Compounding this*, LLMs lack robust self-validation for constraint adherence and reasoning consistency [Bommasani et al., 2022, Chang, 2025], a limitation loosely analogous to Gödel-style barriers [Gödel, 1967] and supported empirically [Hong et al., 2024]. Hence we use cross-family judges, mask agent identity, require span-grounded justifications, and aggregate small judge panels ($K \geq 3$) with reliability weighting; judge-swap and order-swap checks, plus a CRIT-free controller variant, indicate that stopping and weights are not driven by a single evaluator.

3 MACI: Information and Behavior Dials with Measurable Stopping

Goal. Coordinate multiple LLM agents to explore meaningfully and then consolidate on well-supported conclusions with calibrated confidence under a fixed token budget. All notation is defined in Appx. D.

Failures we address.

- *Prior capture*: Single models fixate on high-frequency patterns and confirm early impressions.
- *Majority illusion*: Voting appears strong in multiple choice, but does not test the depth of reasoning or the quality of evidence.
- *Unregulated debate*: Contentiousness drifts, evidence quality is not gated, and stopping is ad hoc.
- *Cost sprawl*: Long chains consume budget without proportional gains.

Design summary. MACI exposes two independent controls. The *information dial* (τ_Q) gates which evidence agents may cite by enforcing a quality threshold. The *behavior dial* (CL) sets contentiousness, instructing agents how aggressively to challenge opponents. A moderator tracks four signals—target-aligned evidence quality (Q), inter-agent disagreement (D_{JS}), support overlap (O), and argument quality (CRIT)—and stops when they plateau jointly. The construction of the target prototype θ used by Q is detailed in Appx. D.1.

3.1 The Control Loop

Algorithm 1 (in Appx. C) shows the three-phase cycle. Agents receive a composite anchor $A^{(t)} = (\psi^{(t)}, CL^{(t)}, \tau_Q^{(t)}, \tau_{CRIT}^{(t)})$ that contains the history of curated debates, current contentiousness instruction, and evidence quality thresholds. Each agent produces claim-justification pairs with probability distribution $p_u^{(t)}$ over the outcomes and evidence cited spans $\hat{\mathcal{E}}_u^{(t)}$. The moderator scores arguments with CRIT (Appendix E), computes evidence quality Q for the cited spans, and admits only those satisfying both gates, $Q \geq \tau_Q(t)$ and $CRIT \geq \tau_{CRIT}(t)$ (defaults in Appx. B.1); it then computes all signals and updates both dials.

3.2 Four Measurement Signals

Notation. Let \mathcal{Y} be finite outcome space, $\Delta(\mathcal{Y})$ the probability simplex. Two agents $u \in \{A, B\}$ alternate over rounds $t = 1, 2, \dots$. Each outputs $p_u^{(t)} \in \Delta(\mathcal{Y})$ and cites evidence spans $\hat{\mathcal{E}}_u^{(t)}$.

Signal 1: Evidence quality (Q). Measures alignment between cited evidence and target distribution using encoder embeddings:

$$Q^{(t)} = \cos(\bar{\mathbf{e}}^{(t)}, \boldsymbol{\theta}), \quad \bar{\mathbf{e}}^{(t)} = \frac{1}{|\mathcal{E}^{(t)}|} \sum_{e \in \mathcal{E}^{(t)}} \frac{\phi(e)}{\|\phi(e)\|}, \quad (1)$$

where $\mathcal{E}^{(t)}$ collects the spans from *admitted* arguments in round t , and $\boldsymbol{\theta}$ is the target prototype. Rising $Q^{(t)}$ indicates convergence on task-relevant evidence.

Admission rule. For each *candidate* argument i at round t , we compute a per-argument evidence score $q_i^{(t)}$ (analogous to (1), using only the spans cited by i). The moderator admits i iff it passes the **dual gate**:

$$q_i^{(t)} \geq \tau_Q(t) \quad \text{and} \quad \text{CRIT}_i^{(t)} \geq \tau_{\text{CRIT}}(t).$$

After admission, $\mathcal{E}^{(t)}$ aggregates all admitted spans and $Q^{(t)}$ summarizes the evidence quality of that batch. Default settings for τ_Q and τ_{CRIT} appear in Appx. B.1.

Signal 2: Disagreement (D_{JS}). Jensen-Shannon divergence quantifies distributional disagreement:

$$D_{\text{JS}}^{(t)} = \frac{1}{2} \text{KL}(p_A^{(t)} \| m^{(t)}) + \frac{1}{2} \text{KL}(p_B^{(t)} \| m^{(t)}), \\ m^{(t)} = \frac{1}{2}(p_A^{(t)} + p_B^{(t)}). \quad (2)$$

D_{JS} is symmetric and bounded in $[0, 1]$ when using log base 2, and remains finite under disjoint support. Falling D_{JS} tracks convergence; plateaus indicate exhausted productive disagreement (thresholds are selected on the development set; Appendix D).

Signal 3: Support overlap (O). Jaccard similarity of cited evidence sets:

$$O^{(t)} = \frac{|\hat{\mathcal{E}}_A^{(t)} \cap \hat{\mathcal{E}}_B^{(t)}|}{|\hat{\mathcal{E}}_A^{(t)} \cup \hat{\mathcal{E}}_B^{(t)}|}. \quad (3)$$

Rising overlap indicates agents grounding arguments in shared evidence rather than talking past each other. Combined with falling D_{JS} , this signals genuine convergence rather than forced agreement.

Signal 4: Argument quality (CRIT). Cross-family LLM evaluator scores each argument on $[0, 1]$ for logical coherence, evidence support, and reasoning depth (Appendix E). The moderator maintains exponential moving average of per-agent quality:

$$\Gamma_u^{(t)} = \lambda \Gamma_u^{(t-1)} + (1 - \lambda) \overline{\text{CRIT}}_{u,t}, \\ \omega_u^{(t)} = \frac{\Gamma_u^{(t)} + \epsilon}{\Gamma_A^{(t)} + \Gamma_B^{(t)} + 2\epsilon}, \quad (4)$$

where $\omega_u^{(t)}$ weights agent u 's beliefs. Rising CRIT indicates improving argument quality; agents producing consistently weak arguments receive less weight in the mixture.

3.3 Dual-Dial Control with Plateau Detection

Information gain. Normalized entropy reduction of reliability-weighted mixture:

$$\hat{I}^{(t)} = \left[\frac{H(p^{(t-1)}) - H(p^{(t)})}{\log |\mathcal{Y}|} \right]_+, \quad p^{(t)} = \sum_u \omega_u^{(t)} p_u^{(t)}. \quad (5)$$

Falling \hat{I} indicates lower returns from continued debate.

Plateau detection via relative progress ratios. Rather than fixed thresholds, we measure progress relative to remaining capacity:

$$r_I^{(t)} = \frac{\text{MA}_w(\hat{I}^{(t)})}{\text{MA}_w(H(p^{(t-1)}) / \log |\mathcal{Y}|) + \eta}, \\ r_D^{(t)} = \frac{\text{MA}_w([D_{\text{JS}}^{(t-1)} - D_{\text{JS}}^{(t)}]_+)}{\text{MA}_w(D_{\text{JS}}^{(t-1)}) + \eta}, \quad (6)$$

where MA_w is length- w moving average, $\eta = 10^{-3}$ prevents division by zero. Binary flags trigger when ratios fall below thresholds for τ_{stop} consecutive rounds:

$$\pi_I^{(t)} = \mathbb{1}[r_I^{(t)} < \varepsilon_I^{\text{rel}}], \quad \pi_D^{(t)} = \mathbb{1}[r_D^{(t)} < \varepsilon_D^{\text{rel}}]. \quad (7)$$

Behavior dial: scheduled contentiousness. When plateaus detected, reduce contentiousness:

$$\text{CL}^{(t+1)} = [\text{CL}^{(t)} - \alpha_I \pi_I^{(t)} - \alpha_D \pi_D^{(t)}]_+. \quad (8)$$

This transitions agents from exploratory ($\text{CL} = 0.9$: “challenge aggressively”) to consolidative ($\text{CL} = 0.5$: “build on agreements”).

Information dial: raising evidence standards. As consensus forms, admit increasingly higher-quality arguments:

$$\tau^{(t+1)} = \min\{\tau^{(t)} + \gamma \pi_I^{(t)}, \tau_{\text{max}} \mathbf{1}\}, \quad \tau^{(t)} = (\tau_Q^{(t)}, \tau_{\text{CRIT}}^{(t)}), \quad (9)$$

where the minimum is applied element-wise, and $\mathbf{1} \in \mathbb{R}^m$ is the all-ones vector for m gates (here $m=2$).

Stopping criterion. Halt when both plateaus persist and evidence quality is sufficient:

$$\sum_{s=0}^{\tau_{\text{stop}}-1} \pi_I^{(t-s)} = \tau_{\text{stop}}, \quad \sum_{s=0}^{\tau_{\text{stop}}-1} \pi_D^{(t-s)} = \tau_{\text{stop}}, \\ Q^{(t)} \geq \tau_Q^{(t)}, \quad O^{(t)} \geq \tau_O. \quad (10)$$

This ensures that the gains have genuinely plateaued, not just temporarily stalled.

Learned scheduler (summary). We replace the fixed (α, γ) schedule with a tiny bandit policy over a discrete action set of $(\Delta\alpha, \Delta\gamma)$ moves, optimizing per-round information gain and dispersion drop under a token budget. Proposition 1 (Appx. L) shows $\tilde{O}(\sqrt{KT})$ no-regret versus the best fixed schedule with zero expected budget violation.

Plateau guarantees (summary). Under a gated averaging update with bounded noise, dispersion $D(t)$ is non-increasing and the plateau controller terminates in $O(1/\varepsilon)$ expected rounds. With a contraction condition the bound becomes $O(\log(1/\varepsilon))$. See Lemma 1 and Proposition 2 (Appx. M).

On dispersion. Our guarantees analyze dispersion as the average KL to the running mixture, $D_{\text{KL}}(t) = \frac{1}{m} \sum_i \text{KL}(p_t^{(i)} \| \bar{p}_t)$, which yields monotonicity under gated averaging by convexity; in plots we additionally report JSD, which is locally Lipschitz-equivalent on the δ -smoothed simplex (Appx. M).

3.4 Initialization Strategy

Before debate, we compute initial evidence quality Q and disagreement D_{JS} from the query and retrieved context. We initialize contentiousness as

$$\text{CL}^{(1)} = \begin{cases} 0.7 & \text{if } Q \geq \tau_Q^{\text{hi}} \text{ and } D_{\text{JS}} \leq \tau_{D_{\text{JS}}}^{\text{lo}}, \\ 0.9 & \text{if } Q \leq \tau_Q^{\text{lo}} \text{ and } D_{\text{JS}} \geq \tau_{D_{\text{JS}}}^{\text{hi}}, \\ 0.8 & \text{otherwise.} \end{cases}$$

The thresholds $\tau_Q^{\text{lo}}, \tau_Q^{\text{hi}}, \tau_{D_{\text{JS}}}^{\text{lo}}, \tau_{D_{\text{JS}}}^{\text{hi}}$ are set by percentiles on the development set (Appendix F). This reduces wasted exploration on straightforward cases while preserving search capacity on ambiguous ones.

3.5 Complete Algorithm

Algorithm 1 integrates all components (see Appx. C for complete pseudocode).

3.6 Problem regime classification

MACI targets open-ended reasoning where (1) the answer space is large ($|\mathcal{Y}| \geq 20$), (2) evidence synthesis is required rather than pattern matching, and (3) uncertainty quantification matters. For small multiple-choice tasks ($|\mathcal{Y}| \leq 5$), majority voting typically suffices. Appendix K.1 formalizes this distinction.

4 Empirical Validation

We evaluate MACI in two domains, clinical diagnosis (G1) and news bias detection (G2), measuring accuracy, calibration, and cost, with ablations and case studies.

4.1 G1: Clinical Diagnosis

Dataset and protocol. **Kaggle Symptom-Disease** [Tharmalingam, 2023]: 1,500 cases across 30 diseases. The corpus provides only current symptoms (no labs or history). We use the *unconstrained* setting: models output free-text diagnoses from 100+

Table 2: Pairwise MACI vs. single models on 1,500 cases. Stars: paired Wilcoxon vs. best single (BH FDR $q=0.05$): *** $p<0.001$, ** $p<0.01$.

Model	Acc@1	Acc@3	MRR
GPT-4o	0.734	0.847	0.781
Claude 3 Opus	0.720	0.832	0.768
Gemini 1.5 Pro	0.693	0.825	0.756
GPT+Claude	0.786***	0.874***	0.823***
GPT+Gemini	0.751**	0.861**	0.807**
Claude+Gemini	0.745***	0.858***	0.798***

possibilities (no candidate list), matching clinical triage with broad differentials.

Why voting fails here. When predictions are constrained to 30 labels, accuracy reaches 95–97%. In the unconstrained regime, agreement collapses and Acc@1 falls to 73–78% because many cases are under-specified and require evidence synthesis rather than pattern matching. Majority voting is unreliable in large output spaces (Appx. K).

Setup. **Backbones:** GPT-4o, Claude 3 Opus, Gemini 1.5 Pro; all pairs ($M=2$). **Retrieval:** BM25 + dense reranking ($k_{\text{ret}}=32$). **Baselines:** best single; majority vote (20); self-consistency (20); fixed-contentiousness debate [Liang et al., 2024]. **Statistics:** BCa 95% CIs from $B=20$ bootstraps; paired Wilcoxon with Benjamini–Hochberg FDR ($q=0.05$).

4.1.1 Main Results, Three Parts

Results #1: MACI vs. single models. Every MACI pair outperforms its best single (Table 2); for example, GPT-4o+Claude improves Acc@1 by +5.2 pp.

Results #2: MACI ablation. MACI relies on three active controls: (i) behavioral scheduling (high CL for exploration, low CL for consolidation), (ii) *dual gating* ($Q \geq \tau_Q$ and $\text{CRIT} \geq \tau_{\text{CRIT}}$), and (iii) information-theoretic stopping (plateaus in D_{JS} and IG). Fixed-contentiousness debate wastes tokens; passive aggregation uses 5–7× more tokens and underperforms. Table 3 shows orthogonal effects: removing the Q gate costs –5.2 pp Acc@1 and raises ECE by +0.040; uniform weights (no reliability) cost –3.0 pp and +0.013 ECE; disabling scheduling (holding CL high/low) costs –3.9 to –6.0 pp with larger ECE.

Table 3: Ablations on clinical diagnosis. Δ is the drop relative to full MACI (lower is better). (Uniform weights = no reliability weighting)

Variant	Acc@1	Δ	ECE	Δ
MACI (full)	77.8	—	0.081	—
No schedule (high)	73.9	3.9	0.112	0.031
No schedule (low)	71.8	6.0	0.099	0.018
No Q gate	72.6	5.2	0.121	0.040
Uniform weights	74.8	3.0	0.094	0.013

Results #3: MACI vs. competing schemes. Against debate/aggregation baselines, MACI is more accurate and better calibrated with fewer tokens (Table 4): +3.9 pp over majority vote and +3.7 pp over Liang et al. (both $p < 0.001$), ECE 0.081 vs. 0.103, and 19% fewer generation tokens. These gains align with the ablation evidence.

Computational overhead. MACI uses 18.4k tokens vs. 6.8k for a single model ($2.7 \times$ overhead). For high-stakes settings where accuracy reduces costly errors, this overhead is justified; for routine tasks, single-model inference may suffice.

Evidence quality stratification. Accuracy correlates with initial Q : cases with $Q > 0.7$ reach 78.3% vs. 69.8% for $Q < 0.3$ (Table 20, Appx. K). This validates Q as a useful signal and suggests retrieval improvements may benefit MACI more than parameter tuning.

Controller guarantee (theory-lite). With bounded noise and gated averaging, dispersion $D(t)$ is non-increasing, and the plateau controller terminates in $O(1/\varepsilon)$ expected rounds; under a contraction, $D(t)$ decays geometrically and termination is $O(\log(1/\varepsilon))$ (Lem. 1, Prop. 2, Cor. 1, Appx. M).

4.1.2 Two Case Studies: Active Control and Information Acquisition

We illustrate MACI’s scheduling and gating, and show termination aligns with plateaued IG and low dispersion. Each case ends with a targeted information-acquisition plan specifying *what to fetch next* for retrieval-augmented generation. Full transcripts appear in Appx. G and H.

Case 1: Dengue vs. Chikungunya (3 rounds). **Symptoms:** skin rash, joint pain, vomiting, fatigue, high fever, headache, retro-orbital pain, myalgia, red spots. **Ground truth:** Dengue Fever.

Table 5 shows scheduling $CL \in \{0.9, 0.7, 0.5\}$. $R1$ ($CL=0.9$): GPT-4o proposes specific viral diagnoses (Dengue 60%, Chikungunya 25%, Zika 15%); Gemini

stays categorical (Viral Infection 60%, Autoimmune 20%, Bacterial 15%). High disagreement ($D_{JS}=0.56$). $R2$ ($CL=0.7$): targeted challenges shift Gemini to Dengue (50%) and Chikungunya (30%); $D_{JS}=0.37$, CRIT $0.75 \rightarrow 0.82$. $R3$ ($CL=0.5$): distributions align (Dengue 60%, Chikungunya 35%, Zika 5%); $D_{JS}=0.02$, MI plateaus (0.49); trigger stop flags.

Figure 1 (internal signals). Fig. 1 shows entropy declining as CL moves from explore to consolidate; Q rising as the gate τ tightens; and CRIT increasing as low-quality arguments are filtered. Dispersion D_{JS} (not shown) falls in parallel; termination matches IG and dispersion plateaus.

Evaluator robustness. Reversing debater order leaves the CRIT winner unchanged; cross-family judge swaps preserve item-level rankings (Appx. E.7).

Informative RAG recommendations. Beyond “Dengue Fever (60%),” MACI outputs a plan: *Questions* (endemic travel; bleeding/bruising), *Labs* (CBC for thrombocytopenia; IgM/IgG; PCR; NS1 antigen), plus retrieval cues for RAG.

Case 2: Hepatitis differential (4 rounds, adaptive stopping). **Symptoms:** itching, vomiting, fatigue, weight loss, high fever, jaundice, dark urine, abdominal pain. **Ground truth:** Hepatitis C.

Table 6 shows $CL \in \{0.9, 0.7, 0.5, 0.3\}$. $R1$ ($CL=0.9$): GPT-4o emphasizes HCV (40%); Claude emphasizes HBV (35%) and alcoholic hepatitis (15%); $D_{JS}=0.22$. $R2$ ($CL=0.7$): reasoning integration; $D_{JS}=0.12$, CRIT rises. $R3$ ($CL=0.5$): near convergence (HCV 35%, HBV 25–30%, cirrhosis 20%); $D_{JS}=0.04$, MI 0.49. $R4$ ($CL=0.3$): distributions nearly identical; termination.

Table 6: Signal evolution: Hepatitis case (4 rounds).

Round	CL	\widetilde{W}_1	MI	CRIT	D_{JS}
1	0.9	0.52	0.39	0.76	0.22
2	0.7	0.45	0.41	0.83	0.12
3	0.5	0.33	0.49	0.89	0.04
4	0.3	0.31	0.49	0.92	0.03
Change		-40%	+26%	+21%	-86%

Internal signals (case view). As in Case 1, entropy declines as CL schedules down; Q and CRIT rise with tighter gates; D_{JS} falls toward zero. Fig. 2 visualizes monotonic dispersion declines for both cases.

Evaluator robustness. The same checks apply: order swap and cross-family judge swap leave outcomes stable (Appx. E.7).

Table 4: Main results (1,500 cases). MACI improves accuracy and calibration with fewer tokens and rounds.

Method	Acc@1	MRR	ECE	Brier	Tokens (10^3)	Rounds
Single best	72.1	0.802	0.126	0.187	6.8	1.0
Majority vote (20)	73.9	0.817	0.139	0.196	92.3	1.0
Self-consistency (20)	74.7	0.827	0.147	0.201	128.6	1.0
Liang et al. [Liang et al., 2024]	74.1	0.834	0.103	0.173	22.6	3.3
MACI (ours)	77.8	0.856	0.081	0.158	18.4	2.7

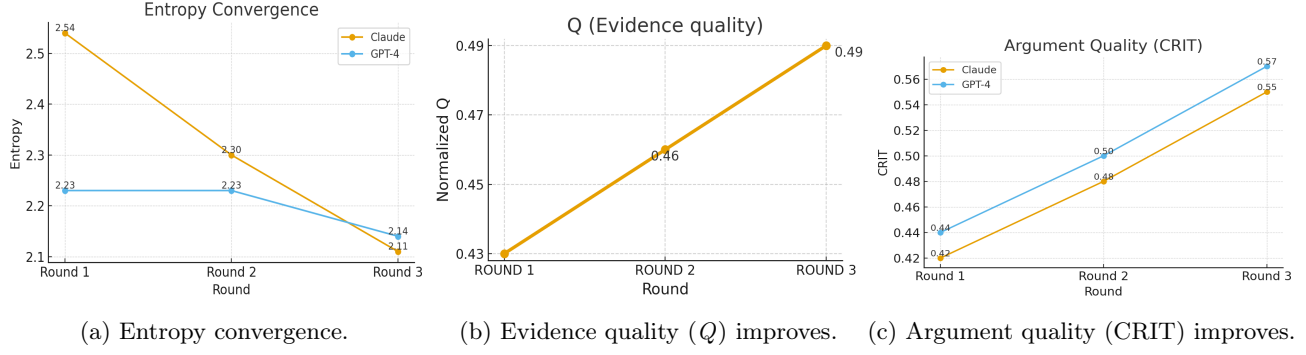


Figure 1: Internal signals over debate rounds (clinical). **Left:** entropy declines under scheduled CL. **Middle:** evidence quality Q rises as the evidence gate τ_Q tightens. **Right:** argument quality CRIT rises as low-quality arguments are filtered. Termination coincides with plateaued IG and low dispersion (not shown).

Table 5: Signal evolution on a Dengue case. \widetilde{W}_1 : Wasserstein-1 distance; MI: mutual information; D_{JS} : Jensen–Shannon divergence. Lower is better for \widetilde{W}_1 and D_{JS} ; higher is better for MI. (Appx D)

Round	CL	\widetilde{W}_1	MI	D_{JS}
1	0.9	0.68	0.43	0.56
2	0.7	0.44	0.46	0.37
3	0.5	0.36	0.49	0.02
<i>Change (R1 → R3)</i>	<i>-47%</i>	<i>+14%</i>		<i>-96%</i>

Informative RAG recommendations. MACI outputs: *Labs* (HAV/HBV/HCV serology; LFTs ALT/AST/bilirubin/alkaline phosphatase; CBC; INR), *Imaging* (abdominal ultrasound), *History* (alcohol/medications, injection drug use, transfusions), *Monitoring* (encephalopathy, coagulopathy).

4.2 G2: News Bias Detection (Cross-Domain)

Why this tests portability. News bias differs from G1 on *evidence* (full articles vs. symptom lists), *labels* (5-point continuous vs. discrete), and *ground truth* (partisan-anchored vs. objective). A self-supervised study maps CL to linguistic patterns across topics (Table 15, Appx. I): high CL=0.9 is confrontational, low CL=0.3 is cooperative. A shallow classifier predicts CL bins with AUC 0.83 (Table 17), indicating measurable behavior modulation beyond domain content.

Dataset and setup. We use 619 scandal articles from [Budak et al., 2016] with Democrat/Republican five-point ratings (−2 to +2). Hyperparameters match G1: CL $\in \{0.9, 0.7, 0.5\}$, gates (τ_Q, τ_O) , and the same stopping rule. Two agents (GPT-4o, Claude 3 Opus) start with asymmetric partisan framings.

Table 7: News bias results (619 articles). *Tokens* are reported in thousands ($\times 10^3$). MAD: mean absolute deviation from centrist (0).

Method	MAD	ECE	Brier	Tokens	Rounds
D-annotator	0.84	0.168	0.221	–	–
R-annotator	0.76	0.173	0.218	–	–
Average (D+R)	0.51	0.142	0.189	–	–
Unscheduled	0.38	0.127	0.178	11.7	3.8
MACI	0.12	0.093	0.167	8.2	2.4

Results #1: Narrowing partisan gaps. Partisan annotators diverge (MAD 0.84 vs. 0.76). Averaging yields 0.51; unscheduled debate 0.38. MACI achieves **0.12** MAD (76% vs. averaging, 68% vs. unscheduled), with better calibration (ECE 0.093 vs. 0.127–0.173) and **30%** fewer tokens (8.2 vs. 11.7). Fig. 3a shows centering between partisan peaks.

Results #2: Which controls matter (ablations). Removing scheduling raises MAD by +0.14–0.19; removing the Q gate by +0.17; uniform (no-reliability) weights by +0.06 and ECE by +0.014 (Table 8).

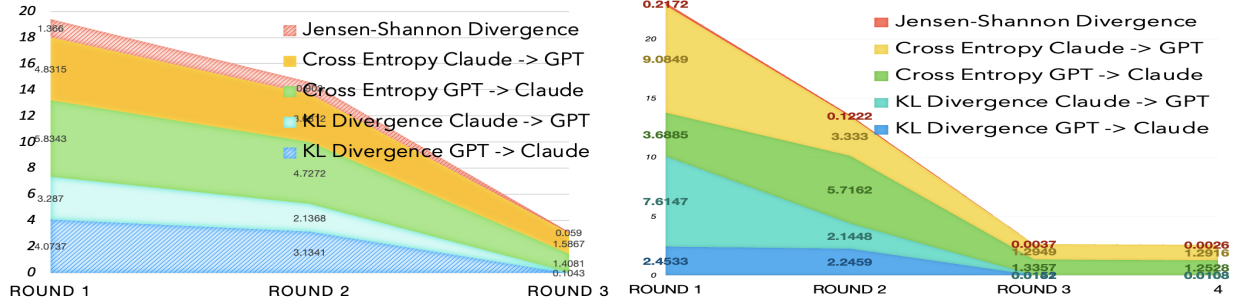


Figure 2: Convergence in two cases: D_{JS} and allied distances decrease monotonically under scheduling.

Table 8: Ablations. Positive Δ MAD indicates worse bias.

Variant	MAD	Δ	ECE	Δ
MACI (full)	0.12	–	0.093	–
No schedule (high)	0.31	0.19	0.134	0.041
No schedule (low)	0.26	0.14	0.118	0.025
No Q gate	0.29	0.17	0.141	0.048
Uniform weights	0.18	0.06	0.107	0.014

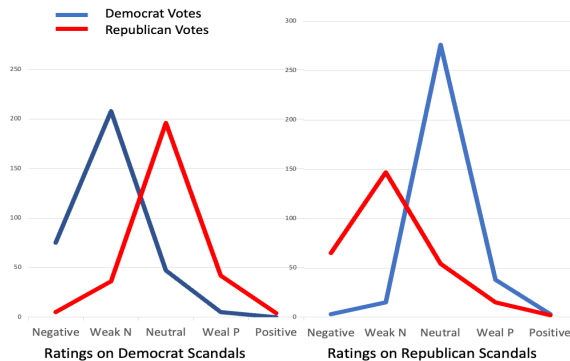


Figure 3: Convergence signals during bias mitigation (news bias). Wasserstein distance falls, normalized MI rises and then plateaus, and cross-entropy declines. Debates stop when dispersion and information gains plateau, mirroring the clinical setting (Appx. J.3).

Results #3: Signal convergence and behavioral transfer. Debates average 2.4 rounds and stop when dispersion and information gains plateau. Convergence traces mirror G1; see Appx. J.3 for signal plots.

Example (one case). On “Christopher Columbus,” one agent begins Euro-centric (expansion and trade) and the other foregrounds indigenous harms. Over four rounds the former acknowledges severe consequences within broader colonial policy and recommends balanced presentation with citations (Table 20, Appx. J.3).

Portability. Same code and hyperparameters, no domain tuning. Controls (CRIT and Q gates, CL schedul-

ing, D_{JS} and O stopping) transfer across evidence types and label structures. Per-article distributions appear in Appx. J.3.

Budget-aware learned scheduler. We also provide a drop-in scheduler that replaces the fixed (α, γ) schedule with a small bandit over $(\Delta\alpha, \Delta\gamma)$ moves, optimizing per-round IG gains and dispersion drops under a token budget. The policy enjoys $\tilde{O}(\sqrt{KT})$ no-regret against the best fixed schedule with zero expected budget violation (Prop. 1, Appx. L). We keep the fixed schedule in G1/G2 main tables for comparability.

5 Conclusion

Advancing multi-agent orchestration. We presented MACI, a control framework that extends contentiousness modulation Chang [2023a,b] with (1) *dual-dial* control separating information admission from behavioral stance, (2) *information-theoretic* stopping via relative progress ratios, and (3) *adaptive* initialization to reduce wasted exploration. Unlike passive aggregation or fixed debate, MACI steers deliberation using measurable signals—disagreement, overlap, evidence quality, and argument quality—and halts when gains plateau.

On clinical diagnosis (1,500 cases), MACI improves accuracy (+3.9 pp over majority vote; +3.7 pp over fixed-contentiousness) and calibration (ECE 0.081 vs. 0.103) while using 19% fewer generation tokens; case studies show convergence (disagreement \downarrow 86–96%, CRIT \uparrow 21–26%). CRIT is order-invariant and stable under cross-family judge swaps (2–3% winner flips; Appx. E.7). Theory-lite guarantees bound dispersion and ensure termination in $O(1/\varepsilon)$ rounds (improving to $O(\log(1/\varepsilon))$), and a budget-feasible UCB scheduler attains $\tilde{O}(\sqrt{KT})$ no-regret with zero expected budget violation (Appx. M, L). News-bias validation (619 articles) shows portability: the same controls reduce the partisan gap by 68% without domain tuning.

Limitations and directions.

- **Scope.** We evaluate two domains with subjective judgment; broader testing on tasks with objective ground truth (math, code, factual QA) and longer chains remains future work. Retrieval quality mediates performance (Sec. 4.1), suggesting gains from stronger evidence acquisition.
- **LLM-judge dependence.** CRIT uses cross-family evaluators and may inherit bias. We mitigate via identity masking, span-grounded justifications, and judge-swap checks (2–3% flips; Appx. E.7). Lower-capability regimes may require larger K , tighter stop tolerances, and periodic human audits.
- **Cost trade-offs.** MACI uses $2.7\times$ tokens vs. single-model inference; while accuracy gains justify overhead for complex cases, domain-specific cost–benefit studies are needed.
- **Hyperparameters.** CL schedules, gates, and plateau tolerances are tuned on dev data; generalization beyond diagnosis/news is open. Scaling to 3–5 agents and meta-learned initialization are natural next steps.

Closed-loop RAG. A promising direction is coupling MACI’s acquisition plans to budgeted RAG with end-to-end evaluation; transcripts (Appx. G, H) enable auditability.

Overall, MACI reframes multi-agent debate as a controllable, auditable, and *provably terminating* controller, turning orchestration from heuristics into a budget-aware, measurable process.

References

R. Bommasani, D. A. Hudson, E. Adeli, R. Altman, and more. On the opportunities and risks of foundation models, 2022. URL <https://arxiv.org/abs/2108.07258>.

T. Brown, B. Mann, N. Ryder, et al. Language models are few-shot learners. *Advances in neural information processing systems*, 33:1877–1901, 2020.

C. Budak, S. Goel, and J. M. Rao. Fair and Balanced? Quantifying Media Bias through Crowdsourced Content Analysis. *Public Opinion Quarterly*, 80(S1): 250–271, 04 2016. doi: 10.1093/poq/nfw007. URL <https://doi.org/10.1093/poq/nfw007>.

M. Cemri, M. Z. Pan, A. Parameswaran, D. Klein, K. Ramchandran, M. Zaharia, J. E. Gonzalez, and I. Stoica. Why Do Multi-Agent LLM Systems Fail?, 2025. URL <https://arxiv.org/abs/2503.13657>. arXiv:2503.13657.

E. Y. Chang. Crit: Prompting large language models with the socratic method. In *IEEE Computing and Communication Workshop and Conference (CCWC)*, 2023a. URL <https://arxiv.org/abs/2303.08769>. arXiv:2303.08769.

E. Y. Chang. Examining GPT-4’s Capabilities and Enhancement with SocraSynth. In *The 10th International Conf. on Comp. Science and Comp. Intelligence*, December 2023b.

E. Y. Chang. *Multi-LLM Agent Collaborative Intelligence: The Path to Artificial General Intelligence*. SocraSynth, March 2024; ACM Books (accepted), 2025.

H. K. Choi, X. Zhu, and Y. Li. Debate or vote: Which yields better decisions in multi-agent large language models?, 2025a. URL <https://arxiv.org/abs/2508.17536>.

S. Choi, C. Y. Park, K. Halmekyt, H. Chung, I. Kim, J. Seo, J. Song, D. Gwak, and Y. Kang. Debate or vote: Which yields better decisions in multi-agent deliberation? *arXiv preprint arXiv:2508.17536*, 2025b. URL <https://arxiv.org/abs/2508.17536>.

M. J. A. N. d. C. Condorcet. *Essai sur l’application de l’analyse à la probabilité des décisions rendues à la pluralité des voix*. De l’Imprimerie Royale, Paris, 1785.

T. M. Cover and J. A. Thomas. *Elements of Information Theory*. Wiley-Interscience, 2nd edition, 2006.

Z. Dai et al. Gpts are gpts: An early look at the labor market impact of large language models. In *arXiv preprint arXiv:2304.09797*, 2023.

A. Estornell and Y. Liu. Multi-llm debate: Framework, principles, and interventions. In *Advances in Neural Information Processing Systems 37 (NeurIPS)*, 2024.

K. Gödel. On formally undecidable propositions of *Principia Mathematica* and related systems i. In J. van Heijenoort, editor, *From Frege to Gödel: A Source Book in Mathematical Logic, 1879–1931*, pages 596–616. Harvard University Press, 1967. Translated by Jean van Heijenoort.

G. Hong et al. Mixtures of in-context learners. In *Proceedings of the 63rd Annual Meeting of the Association for Computational Linguistics (ACL)*, Bangkok, Thailand, 2025. Association for Computational Linguistics. URL <https://aclanthology.org/2025.acl-long.1277/>.

R. Hong, H. Zhang, X. Pang, D. Yu, and C. Zhang. A Closer Look at the Self-Verification Abilities of Large Language Models in Logical Reasoning. *arXiv:2311.07954*, 2024. URL <https://arxiv.org/abs/2311.07954>.

G. Irving, P. Christiano, and D. Amodei. AI safety via debate. *arXiv:1805.00899*, 2018. URL <https://arxiv.org/abs/1805.00899>.

L. V. Kantorovich. On the translocation of masses. *Doklady Akademii Nauk*, 37(7-8):199–201, 1942.

J. Kaplan, S. McCandlish, T. Henighan, et al. Scaling laws for neural language models. *arXiv preprint arXiv:2001.08361*, 2020.

Z. Kenton, N. Y. Siegel, J. Kramár, J. Brown-Cohen, S. Albanie, J. Bulian, R. Agarwal, D. Lindner, Y. Tang, N. D. Goodman, and R. Shah. On scalable oversight with weak llms judging strong llms. *arXiv preprint arXiv:2407.04622*, 2024. URL <https://arxiv.org/abs/2407.04622>.

S. Kullback. *Information Theory and Statistics*. John Wiley & Sons, 1951.

W. Li, Y. Lin, M. Xia, and C. Jin. Rethinking mixture-of-agents: Is mixing different large language models beneficial?, 2025. URL <https://arxiv.org/abs/2502.00674>.

T. Liang, Z. He, W. Jiao, X. Wang, and more. Encouraging divergent thinking in large language models through multi-agent debate. In *Proceedings of the 2024 Conference on Empirical Methods in Natural Language Processing*, pages 17889–17904, Nov. 2024. doi: 10.18653/v1/2024.emnlp-main.992. URL [https://aclanthology.org/2024.emnlp-main.992/](https://aclanthology.org/2024.emnlp-main.992).

J. Lin. Divergence measures based on the shannon entropy. *IEEE Transactions on Information theory*, 37(1):145–151, 1991.

Y. Liu, J. Cao, Z. Li, R. He, and T. Tan. Breaking mental set to improve reasoning through diverse multi-agent debate. In *International Conference on Learning Representations (ICLR)*, 2025.

A. Panickssery, S. R. Bowman, and S. Feng. LLM evaluators recognize and favor their own generations. In *Advances in Neural Information Processing Systems 37 (NeurIPS 2024)*, 2024. URL <https://neurips.cc/virtual/2024/poster/96672>.

B. Recht. A tour of reinforcement learning: The view from continuous control. *Annual Review of Control, Robotics, and Autonomous Systems*, 2:253–279, 2019.

B. Settles. Active learning literature survey. Technical Report 1648, University of Wisconsin-Madison Department of Computer Sciences, 2009.

C. E. Shannon. A mathematical theory of communication. *Bell System Technical Journal*, 27(3):379–423, 1948.

J. E. Shore and R. W. Johnson. Axiomatic derivation of the principle of maximum entropy and the principle of minimum cross-entropy. *IEEE Transactions on Information Theory*, 26(1):26–37, 1980.

A. P. Smit, P. Duckworth, N. Grinsztajn, T. D. Barrett, and A. Pretorius. Should we be going MAD? a look at multi-agent debate strategies for llms. In *Proceedings of the 41st International Conference on Machine Learning (ICML 2024)*, volume 235 of *Proceedings of Machine Learning Research*, pages 49941–49956. PMLR, 2024. URL <https://proceedings.mlr.press/v235/smit24a.html>.

L. Tharmalingam. Kaggle Disease Symptoms and Patient Profile Dataset, 2023. URL <https://www.kaggle.com/code/rospel/basic-medical-info-a-key-to-predict-disease>.

A. Vaswani et al. Attention is all you need. *Advances in neural information processing systems*, 2017.

J. von Oswald, E. Niklasson, E. Randazzo, J. Sacramento, A. Mordvintsev, A. Zhmoginov, and M. Vladymyrov. Transformers learn in-context by gradient descent. In *Proceedings of the 40th International Conference on Machine Learning, ICML’23*, pages 35151–35174, 2023.

J. Wang, J. Wang, B. Athiwaratkun, C. Zhang, and J. Zou. Mixture-of-agents enhances large language model capabilities. *arXiv:2406.04692*, 2024a. URL <https://arxiv.org/abs/2406.04692>.

Q. Wang, Z. Wang, Y. Su, H. Tong, and Y. Song. Rethinking the bounds of llm reasoning: Are multi-agent discussions the key? In *Proceedings of the 62nd Annual Meeting of the Association for Computational Linguistics (ACL 2024)*, pages 6106–6131, 2024b. doi: 10.18653/v1/2024.acl-long.331. URL <https://aclanthology.org/2024.acl-long.331>.

S. Wang, C.-H. H. Yang, J. Wu, and C. Zhang. Bayesian example selection improves in-context learning for speech, text and visual modalities. In *Proceedings of the 2024 Conference on Empirical Methods in Natural Language Processing (EMNLP)*, pages 20812–20828, 2024c. doi: 10.18653/v1/2024.emnlp-main.1158. URL <https://aclanthology.org/2024.emnlp-main.1158.pdf>.

X. Wang, J. Wei, D. Schuurmans, Q. Le, E. Chi, S. Narang, A. Chowdhery, and D. Zhou. Self-consistency improves chain of thought reasoning in language models. In *ICLR*, 2023. URL <https://arxiv.org/abs/2203.11171>.

S. M. Xie, A. Raghunathan, P. Liang, and T. Ma. An explanation of in-context learning as implicit bayesian inference. *International Conference on Learning Representations (ICLR)*, 2022.

Appendix Overview

- **Appendix A:** Notation and symbols
- **Appendix B:** Configuration, hyperparameters, experimental setup
- **Appendix C:** MACI algorithm specification
- **Appendix D:** Information-theoretic signals
- **Appendix E:** CRIT evaluator details
- **Appendix F:** Adaptive initialization strategy
- **Appendix G:** Dengue case study (full transcript)
- **Appendix H:** Hepatitis case study (full transcript)
- **Appendix I:** Linguistic analysis and behavioral validation
- **Appendix J:** News bias detection
- **Appendix K:** Majority vote failure analysis
- **Appendix L:** Learned scheduler for (α, γ) (algorithm and no-regret analysis)
- **Appendix M:** Plateau guarantees (monotone dispersion and termination)

A Notation and Symbols

Table 9: Key symbols used throughout.

Symbol	Meaning
MACI	Multi-Agent Collaborative Intelligence (dual-dial control framework)
Q	Target-aligned evidence quality
D_{JS}	Inter-agent disagreement (Jensen-Shannon divergence)
O	Support overlap (Jaccard over cited spans)
\hat{I}	Normalized information gain (entropy drop)
CRIT	Argument-quality score from independent LLMs
CL	Behavior dial (contentiousness level)
τ_Q	Evidence-quality gate (information dial)
τ_{CRIT}	Argument-quality gate (evaluator dial)
τ_O	Overlap floor used only in the stopping rule
$\omega_u^{(t)}$	Reliability weights (EMA of CRIT), agent u
$p_u^{(t)}$	Agent u 's probability distribution at round t
$p^{(t)}$	Reliability-weighted mixture distribution
$\mathcal{E}_u^{(t)}$	Evidence spans cited by agent u at round t
$r_I^{(t)}, r_D^{(t)}$	Relative progress ratios (information gain, disagreement)
$\pi_I^{(t)}, \pi_D^{(t)}$	Plateau detection flags
\tilde{W}_1	Normalized Wasserstein-1 distance

B Configuration and Hyperparameters

B.1 Default Hyperparameters

Unless specified otherwise, MACI uses these settings across all experiments:

Control parameters.

- **Reliability smoothing (EMA):** $\lambda = 0.8$, $\epsilon = 10^{-6}$.
- **Initial gates:** $\tau_Q^{(1)} = 0.50$, $\tau_{CRIT}^{(1)} = 0.30$.
- **Gate tightening:** $(\tau_Q^{(t+1)}, \tau_{CRIT}^{(t+1)}) \leftarrow \min\{(\tau_Q^{(t)}, \tau_{CRIT}^{(t)}) + \gamma \pi_I^{(t)}, (\tau_{\max}, \tau_{\max})\}$.
- **Overlap floor for stopping (not an admission gate):** $\tau_O = 0.30$.

Initialization bins (development set).

- High quality ($Q \geq 0.7$) and low disagreement ($D_{JS} \leq 0.3$): $CL^{(1)} = 0.7$.
- Low quality ($Q \leq 0.5$) and high disagreement ($D_{JS} \geq 0.5$): $CL^{(1)} = 0.9$.
- Otherwise: $CL^{(1)} = 0.8$.

Contentiousness schedule. Standard progression: $CL \in \{0.9, 0.7, 0.5, 0.3\}$ with adaptive transitions triggered by plateau flags.

B.2 Clinical Diagnosis (G1) Setup

Dataset. Kaggle Symptom-Disease Corpus, stratified split: 1,500 test cases (50 per disease, 30 conditions). Train/dev/test files and random seeds provided in supplement.

Retrieval. BM25 with dense reranker (all-MiniLM-L6-v2), $k_{\text{ret}} = 32$, max context 4k tokens.

Backbones.

- GPT-4o (gpt-4o-2024-08-06)
- Claude 3 Opus (claude-3-opus-20240229)
- Gemini 1.5 Pro (gemini-1.5-pro-001)
- Temperature: 0.7 for all agents

Evaluation. 20 bootstrap resamples for confidence intervals. BCa method. Paired Wilcoxon tests with Benjamini-Hochberg FDR correction at $q = 0.05$.

B.3 News Bias (G2) Setup

Dataset. 619 scandal-focused articles with partisan annotations (5-point scale). [Budak et al., 2016] collected 803,146 articles from fifteen U.S. news outlets, identifying 10,502 political articles. We focus on scandals as this content exhibits the strongest partisan disagreement.

Agents. GPT-4o and Claude 3 Opus with asymmetric initialization (one Democrat-framed, one Republican-framed).

Identical hyperparameters. Same CL schedule, gates, stopping criteria as G1. No domain-specific tuning.

C MACI Algorithm Specification

Algorithm 1 MACI Moderator with Dual-Dial Control

```

1: Initialize debate record  $\psi^{(1)}$ ; set  $CL^{(1)}$  via dev binning; set
   gates  $\tau_Q^{(1)} = 0.5$ ,  $\tau_{\text{CRIT}}^{(1)} = 0.3$ .
2: for  $t = 1, 2, \dots$  do
3:   Provide  $A^{(t)} = (\psi^{(t)}, CL^{(t)}, \tau_Q^{(t)}, \tau_{\text{CRIT}}^{(t)})$  to both agents.
4:   for  $u \in \{A, B\}$  do
5:     Agent  $u$  emits claim-justification pairs,  $p_u^{(t)} \in \Delta(\mathcal{Y})$ ,
       cites  $\hat{\mathcal{E}}_u^{(t)}$ .
6:   end for
7:   Admission (dual gate). For each candidate argument  $i$  from either agent, compute a per-argument evidence
      score  $q_i^{(t)}$  (analogous to Eq. (1), using only spans cited
      by  $i$ ) and its  $\text{CRIT}_i^{(t)}$ .
8:   Admit  $i$  into  $\psi^{(t+1)}$  iff  $q_i^{(t)} \geq \tau_Q^{(t)}$  and  $\text{CRIT}_i^{(t)} \geq \tau_{\text{CRIT}}^{(t)}$ ;
      otherwise discard.
9:   Update reliability:  $\Gamma_u^{(t)} \leftarrow \lambda \Gamma_u^{(t-1)} + (1 - \lambda) \overline{\text{CRIT}}_{u,t}$ ;
      compute  $\omega_u^{(t)}$  via Eq. (4).
10:  Form mixture:  $p^{(t)} = \sum_u \omega_u^{(t)} p_u^{(t)}$ ; compute  $\hat{I}^{(t)}$  via
      Eq. (5).
11:  Compute signals:  $D_{\text{JS}}^{(t)}$  (Eq. 2),  $O^{(t)}$  (Eq. 3),  $Q^{(t)}$  (Eq. 1).
12:  Update progress ratios  $r_I^{(t)}$ ,  $r_D^{(t)}$  and flags  $\pi_I^{(t)}$ ,  $\pi_D^{(t)}$  via
      Eqs. (6)–(7).
13:  Update dials:  $CL^{(t+1)}$  via Eq. (8); apply Eq. (9) componentwise to obtain  $\{\tau_Q^{(t+1)}, \tau_{\text{CRIT}}^{(t+1)}\}$ .
14:  if stopping criterion Eq. (10) satisfied then
15:    return calibrated  $p^{(t)}$  and curated debate record  $\psi^{(t)}$ .
16:  end if
17: end for

```

Default hyperparameters: $w=3$, $\eta=10^{-3}$, $\lambda=0.8$, $\epsilon=10^{-6}$, $\tau_{\text{stop}}=2$, $\alpha_I=\alpha_D=0.2$, $\gamma=0.1$, $\tau_Q^{(1)}=0.50$, $\tau_{\text{CRIT}}^{(1)}=0.30$.

D Information-Theoretic Signals for Debate Evaluation

This appendix presents the mathematical foundations underlying MACI’s measurement and control framework. We detail each metric’s properties, computational requirements, and specific role in debate moderation.

D.1 Target prototype construction (θ)

D.2 Metric Selection and Usage in MACI

We highlight each metric’s properties and how MACI employs them in practice:

- Cross-Entropy (CE).** Likelihood surrogate that mixes uncertainty and mismatch [Shore and Johnson, 1980, Cover and Thomas, 2006]. *MACI use:* reporting and ablation studies, calibration assessment—not a primary control signal due to asymmetry and sensitivity to probability shifts.
- Entropy.** Quantifies uncertainty in a single prediction [Shannon, 1948]. *MACI use:* per-round *information gain* via normalized entropy reduction of the reliability-weighted aggregate.
- Kullback–Leibler (KL) divergence.** Directed discrepancy measure that is asymmetric and support-sensitive [Kullback, 1951, Cover and Thomas, 2006]. *MACI use:* auxiliary analysis to detect directional belief shifts; not the primary disagreement metric due to asymmetry concerns in symmetric debate settings.
- Jensen–Shannon (D_{JS}) divergence.** Symmetric, bounded $[0,1]$, and finite even under disjoint support; $\sqrt{D_{\text{JS}}}$ satisfies triangle inequality, forming a true metric [Lin, 1991]. *MACI use:* primary *disagreement* signal for discrete labels via unified distance measure $D^{(t)}$.
- Mutual Information (MI) and Normalized MI.** Measures shared information between random variables [Cover and Thomas, 2006]; text-based MI estimators can exhibit high variance. *MACI use:* logged for analysis and visualization; excluded from control loop due to estimation instability.
- Wasserstein Distance (WD).** Geometry-aware discrepancy that respects label structure; efficiently computable in 1D via cumulative distribution functions [Kantorovich, 1942]. *MACI use:* disagreement measurement for ordered or structured outputs via unified distance measure $D^{(t)}$.
- Information Gain (IG).** Entropy reduction of the reliability-weighted mixture, normalized by $\log |\mathcal{Y}|$ for interpretability [Cover and Thomas, 2006]. *MACI use:* primary convergence signal with moving average plateau detection.

D.3 Integration in MACI Framework

MACI employs these signals in three distinct capacities:

Primary Control Signals. The unified distance measure $D^{(t)}$ adapts to output type: $D^{(t)} := D_{JS}(\{B_i^{(t)}\})$ for categorical labels and $D^{(t)} := \widetilde{W}_1(\{B_i^{(t)}\})$ for structured outputs. This provides consistent plateau detection logic while respecting task-appropriate geometry.

Progress Tracking. Normalized information gain $\widehat{I}^{(t)}$ with moving average MA_w quantifies uncertainty resolution. Plateau detection ($\Delta\widehat{I}^{(t)} < \varepsilon_I$ for τ_{stop} rounds) triggers contentiousness reduction: $CL^{(t+1)} = [CL^{(t)} - \alpha_I]_+$.

Analysis and Validation. KL divergence reveals directional bias in agent updates. Mutual information tracks shared representational structure. Cross-entropy supports calibration assessment. These signals inform post-hoc analysis but don't participate in real-time control.

D.4 Mathematical Formulations

Normalized Information Gain

$$\widehat{I}^{(t)} := \frac{H(p^{(t-1)}) - H(p^{(t)})}{\log |\mathcal{Y}|}, \quad p^{(t)} = \sum_u \omega_u^{(t)} p_u^{(t)}.$$

Moving Average Plateau Detection

$$\Delta\widehat{I}^{(t)} := MA_w(\widehat{I}^{(t)}) - MA_w(\widehat{I}^{(t-1)})$$

where $MA_w(x^{(t)}) = \frac{1}{w} \sum_{i=0}^{w-1} x^{(t-i)}$ is the length- w moving average.

Jensen-Shannon Divergence

$$D_{JS}(P, Q) = \frac{1}{2} D_{KL}(P\|M) + \frac{1}{2} D_{KL}(Q\|M),$$

$$M = \frac{1}{2}(P + Q).$$

Normalized Wasserstein Distance For cumulative distribution functions F_P and F_Q :

$$\widetilde{W}_1(P, Q) = \frac{W_1(P, Q)}{\max_{P', Q'} W_1(P', Q')}.$$

Unified Distance Measure

$$D^{(t)} = \begin{cases} D_{JS}(\{B_i^{(t)}\}_{i=1}^M) & \text{categorical labels} \\ \widetilde{W}_1(\{B_i^{(t)}\}_{i=1}^M) & \text{structured labels} \end{cases}$$

D.5 Control Logic and Termination

Contentiousness Reduction. Define $[x]_+ := \max(0, x)$. Two plateau monitors trigger intensity reduction:

$$\text{IG plateau: } \Delta\widehat{I}^{(t)} < \varepsilon_I$$

$$\text{for } \tau_{stop} \text{ rounds} \Rightarrow CL^{(t+1)} = [CL^{(t)} - \alpha_I]_+ \quad (11)$$

$$\text{Dispersion plateau: } |D^{(t)} - D^{(t-1)}| < \varepsilon_D$$

$$\text{for } \tau_{stop} \text{ rounds} \Rightarrow CL^{(t+1)} = [CL^{(t)} - \alpha_D]_+ \quad (12)$$

Termination Criteria. Debate stops when the Eq. (10) plateau conditions hold (for τ_{stop} rounds); we also stop early on budget exhaustion or sustained low CRIT (validator stalemate).

- IG plateau: $\Delta\widehat{I}^{(t)} < \varepsilon_I$ for τ_{stop} rounds
- Dispersion stabilization: $|D^{(t)} - D^{(t-1)}| < \varepsilon_D$ for τ_{stop} rounds
- Budget exhaustion: token/time limits reached
- Validator stalemate: CRIT quality below threshold for extended period

D.6 Practical Interpretation Guidelines

Typical Value Ranges and Decision Thresholds. Based on empirical analysis across clinical reasoning and synthesis tasks:

- **D_{JS} values:** > 0.3 indicates substantial disagreement warranting continued debate; < 0.1 suggests near-consensus
- **Information Gain:** Normalized values > 0.1 indicate meaningful uncertainty reduction; < 0.02 suggests convergence plateau
- **Wasserstein Distance:** Interpretation depends on label structure; focus on relative changes rather than absolute values
- **CRIT scores:** Socratic evaluation yields $[0,1]$ range; typical threshold $\tau = 0.3$

Default Hyperparameters. Standard settings: $w = 3$ (moving average window), $\tau_{stop} = 2$ (plateau detection), $\varepsilon_I = 0.02$, $\varepsilon_D = 0.05$, $\alpha_I = \alpha_D = 0.2$ (reduction rates).

E CRIT: Cross-Family Argument Quality Evaluator

E.1 Design Principles

CRIT uses a cross-family LLM evaluator (a different model family than the debating agents) to score argument quality in $[0, 1]$, mitigating self-preference bias [Panickssery et al., 2024] and following the Socratic evaluation protocol Chang [2023a].

Evaluation criteria. Each argument is rated on three equally weighted dimensions ($w_c = 1/3$):

1. **Evidence support:** claims backed by cited spans;
2. **Logical coherence:** valid, non-contradictory reasoning;
3. **Query relevance:** directly addresses the task.

Scoring process. Given debate snippet d with claim Ω , supporting reasons R , and opposing reasons R' : (1) validate each link $r \Rightarrow \Omega$ with quality $\gamma_r \in [0, 1]$; (2) aggregate to a composite $\Gamma = \sum_c w_c \cdot \text{score}_c$; (3) return Γ with a brief justification.

E.2 Multi-Evaluator Aggregation

With K evaluators (default $K=3$) and $N_{u,t}$ arguments from agent u in round t ,

$$\overline{\text{CRIT}}_{u,t} = \frac{1}{N_{u,t}K} \sum_{i=1}^{N_{u,t}} \sum_{k=1}^K s_{u,t,i}^{(k)},$$

where $s_{u,t,i}^{(k)}$ is judge k 's composite score for argument i . The round-level score is

$$\text{CRIT}^{(t)} = \frac{1}{N_t K} \sum_u \sum_{i=1}^{N_{u,t}} \sum_{k=1}^K s_{u,t,i}^{(k)}, \quad N_t = \sum_u N_{u,t}.$$

Using $K \geq 3$ reduces single-judge variance; on our development sets we observe Krippendorff's $\alpha \approx 0.68$.

E.3 Reliability Weighting in MACI

Exponential moving average tracks per-agent quality:

$$\Gamma_u^{(t)} = \lambda \Gamma_u^{(t-1)} + (1-\lambda) \overline{\text{CRIT}}_{u,t}, \quad \Gamma_u^{(0)} = 0.5, \quad \lambda = 0.8.$$

Normalized mixture weights with stabilizer $\epsilon = 10^{-6}$:

$$\omega_u^{(t)} = \frac{\Gamma_u^{(t)} + \epsilon}{\sum_v (\Gamma_v^{(t)} + \epsilon)},$$

and the final mixture is $p^{(t)}(y) = \sum_u \omega_u^{(t)} p_u^{(t)}(y)$. Removing reliability weighting (uniform $\omega_u = 0.5$) costs -2.0 pp Acc@1 (Table 3).

E.4 Implementation Details

Evaluator selection. Use a skeptical, diversity-seeking judge from a different model family: (i) for GPT-4o + Claude pairs, use Gemini 1.5 Pro as evaluator; (ii) for Gemini pairs, use Claude 3 Opus as evaluator; temperature 0.3.

Independence. Judges see only the argument text and minimal task context. Agent identity and opponent text are masked. Items are randomized per round.

Quality gate. Arguments are rejected unless $Q \geq \tau_Q(t)$ and $\text{CRIT} \geq \tau_{\text{CRIT}}(t)$; both gates tighten as CL is reduced (Eq. 9).

E.5 Example Scoring

Clinical diagnosis prompt:

Rate this medical argument (0-1 scale):
 Claim: “Bilateral small-joint arthralgia favors Chikungunya over Dengue.”
 Evidence: [Cites CDC arboviral guidelines 2024]
 Reasoning: Joint pain pattern is more severe and prolonged in Chikungunya.
 Score each: Evidence support, Logical coherence, Query relevance.

Evaluator response:

Evidence: 0.90 (authoritative source cited)
 Logic: 0.85 (valid differential reasoning)
 Relevance: 1.00 (directly addresses diagnosis)
 Composite: 0.92

E.6 Hyperparameters

Defaults: $K=3$, $\lambda=0.8$ (EMA), $\epsilon=10^{-6}$, judge temp = 0.3, $w_c=\frac{1}{3}$, $\tau_Q^{(1)}=0.5$, $\tau_{\text{CRIT}}^{(1)}=0.3$.

E.7 CRIT Reliability and Role in MACI

Protocol. We adopt the CRIT evaluator with cross-family judges, identity masking, and span-grounded scoring, following the Socratic protocol. We tune on a disjoint development split and validate on a held-out set of 150 clinical-debate arguments. Judges see only the argument text, cited spans, and minimal task context. Each judge returns three sub-scores (evidence support, logical coherence, query relevance) and a composite in $[0, 1]$ with equal weights. Unless noted, 95% confidence intervals (CIs) for means are computed by nonparametric bootstrap (10,000 resamples). Proportion CIs use the Wilson method. For rank correlations we report bootstrap CIs on Fisher- z transformed coefficients.

Inter-rater agreement. We compute pairwise Pearson and Spearman correlations across all judge pairs, and Krippendorff's α for overall reliability. Table 10 shows $\alpha=0.68$ with strong pairwise correlations (Pearson 0.71 ± 0.05 , Spearman 0.69 ± 0.04). This level is

acceptable for research use, so we employ CRIT conservatively downstream.

Judge-swap stability ($n=100$). We swap the primary judge family (for example, replace Gemini with Claude) on $n=100$ debates and recompute winner rankings. Depending on tie-handling for near-equal scores, the number of winner flips is either (i) $k=2 \Rightarrow 2.0\%$ (Wilson 95% CI [0.55%, 7.00%]) or (ii) $k=3 \Rightarrow 3.0\%$ (Wilson 95% CI [1.03%, 8.45%]). In flipped cases, score margins are small (typical $|\Delta| \approx 0.06$, range [0.04, 0.08]), consistent with near-threshold items rather than systematic bias.

Order invariance ($n=50$). We reverse debater presentation order ($A \rightarrow B$ becomes $B \rightarrow A$) for $n=50$ arguments. The mean absolute score difference is 0.038 (SD 0.024), with 94% of cases showing $|\Delta| < 0.05$. Spearman rank correlation between forward and reverse orders is 0.92 (95% CI [0.87, 0.95]).

Table 10: CRIT reliability on 150 validation arguments with $K=3$ cross-family judges. Means use bootstrap 95% CIs; proportions use Wilson CIs. Judge-swap reports both $k=2$ and $k=3$ outcomes for $n=100$.

Metric	Value	95% CI
<i>Inter-rater agreement</i>		
Krippendorff's α	0.68	[0.63, 0.73]
Pearson (avg pairwise)	0.71	[0.66, 0.76]
Spearman (avg pairwise)	0.69	[0.64, 0.74]
<i>Judge-swap stability ($n=100$)</i>		
Winner-flip rate ($k=2$ of $n=100$)	2.0%	[0.55%, 7.00%]
Winner-flip rate ($k=3$ of $n=100$)	3.0%	[1.03%, 8.45%]
<i>Order invariance ($n=50$)</i>		
Mean $ \text{score}(A \rightarrow B) - \text{score}(B \rightarrow A) $	0.038	[0.031, 0.045]
Spearman rank correlation	0.92	[0.87, 0.95]
Cases with $ \Delta < 0.05$	94%	[88%, 98%]

Usage in MACI. Given these properties, we use CRIT in two conservative roles: (i) *soft aggregation weights* for agent synthesis via $\omega_u^{(t)}$ in Section E and (ii) a component of a *compound stop rule*. Let $\bar{\Gamma}_t$ be the mean CRIT score at round t and Var_t its across-judge variance. We stop when

$$\text{Var}_t < \varepsilon \quad \text{and} \quad |\bar{\Gamma}_t - \bar{\Gamma}_{t-1}| < \delta,$$

for two consecutive rounds, with small thresholds ε, δ selected on a development split. This couples evaluator stability with diminishing returns and prevents over-debating.

Limitations. CRIT relies on LLM evaluators that may exhibit unknown biases or failure modes. Cross-family judging, identity masking, and span grounding

mitigate these risks but do not eliminate them. Systematic validation against human experts remains important future work, especially for high-stakes deployment.

Finally, our stability estimates likely depend on judge competence: using high-capability, cross-family LLMs to assess rubric-based “reasonableness” contributes to the observed robustness, whereas weaker or poorly aligned judges may not yield comparable results; in such settings we recommend increasing K , tightening ε and δ in the stop rule, and adding periodic human audits.

F Adaptive Initialization Strategy

Before debate, we compute two signals from query and retrieved context:

Initial evidence quality. Cosine similarity between mean retrieved embedding and target prototype:

$$Q_0 = \cos(\bar{\mathbf{e}}^{(0)}, \boldsymbol{\theta}), \quad \bar{\mathbf{e}}^{(0)} = \frac{1}{|\mathcal{E}^{(0)}|} \sum_{e \in \mathcal{E}^{(0)}} \frac{\phi(e)}{\|\phi(e)\|}$$

where $\mathcal{E}^{(0)}$ is the initial retrieved evidence set and $\boldsymbol{\theta}$ is the task-specific target prototype.

Initial disagreement. Jensen-Shannon divergence between agents' initial single-pass predictions:

$$D_{JS,0} = \frac{1}{2} \text{KL}(p_A^{(0)} \| m^{(0)}) + \frac{1}{2} \text{KL}(p_B^{(0)} \| m^{(0)}),$$

$$m^{(0)} = \frac{1}{2}(p_A^{(0)} + p_B^{(0)})$$

F.1 Initialization Policy

We bin $(Q_0, D_{JS,0})$ on development set and map to starting parameters:

Intuition. Cases with high-quality evidence and low initial disagreement likely converge quickly, so start with lower contentiousness. Cases with poor evidence quality and high disagreement need more exploration, so start with higher contentiousness.

Evidence gate. Initial gate $\tau^{(1)} = 0.3$ for all cases. Gate rises during debate via Eq. (9) in Section 3.

F.2 Robustness

This simple binning strategy is stable across:

- Encoder layer choice (late layers preferred)
- Pooling method (mean vs. last-token)
- Retrieval depth ($k_{\text{ret}} \in \{16, 32, 48\}$)

Condition	CL ⁽¹⁾	Rationale
High $Q_0 (> P_{70})$, Low $D_{JS,0} (< P_{30})$	0.7	High-quality, low disagreement
Middle range	0.8	Moderate complexity
Low $Q_0 (< P_{30})$, High $D_{JS,0} (> P_{70})$	0.9	Low-quality, high disagreement

Table 11: Development-set percentile bins for initialization. P_X denotes X th percentile.

Percentiles computed once on disjoint development split. After initialization, all parameter updates use live signals ($Q^{(t)}$, $D_{JS}^{(t)}$, $O^{(t)}$, CRIT^(t)) as described in Section 3.

G Detailed MACI Case Study: Dengue vs. Chikungunya Diagnosis

G.1 Three-Phase Debate Walkthrough and Results

This appendix provides a complete case from the medical validation (Section 4.1), showing how MACI’s contentiousness scheduling (CL) and convergence control yield collaborative synthesis. Signals, weighting, and stop rules follow **Algorithm 1**.

Case overview. Two heterogeneous agents (**GPT-4o**, **Gemini 1.5 Pro**) jointly diagnose a patient with: skin rash, joint pain, vomiting, fatigue, high fever, headache, nausea, loss of appetite, retro-orbital pain, back pain, malaise, myalgia, and red spots. Ground truth: *Dengue Fever*. The debate follows $CL \in \{0.9, 0.7, 0.5\}$ and terminates adaptively via the relative plateau rule.

The case exhibits MACI’s three-phase trajectory (exploration → integration → consolidation). Information-theoretic evolution is summarized below (weighted JSD across agent beliefs; normalized 1-Wasserstein \bar{W}_1 between mixtures $p^{(t)}$).

Table 12: Signal evolution during MACI-orchestrated Dengue vs. Chikungunya diagnosis.

Round	CL	\bar{W}_1	MI	CRIT	JSD
1	0.9	0.68	0.43	0.75	0.56
2	0.7	0.44	0.46	0.82	0.37
3	0.5	0.36	0.49	0.87	0.02
Change (%)	-47%	+14%	+16%	-96%	

Adaptive termination. The relative dispersion ratio satisfies $\max_{0 \leq s < \tau} r_D^{(3-s)} < \varepsilon_D^{\text{rel}}$, so the controller stops after Round 3 (Section 3); CL scheduling thus runs only as long as capacity-to-go remains.

G.2 Complete Debate Transcript (Round by Round)

Transcript purpose. We provide complete agent dialogue for transparency and reproducibility. Linguistic analysis in Section G.3 demonstrates how CL modulation produces observable behavioral changes in agent communications.

Readers primarily interested in results may skip to Section G.3 for the pattern analysis.

Note on metrics: The transcript below reports **WD** (raw Wasserstein-1) and D_{JS} as originally logged. In the main text we report *normalized* \bar{W}_1 and weighted D_{JS} ; magnitudes may differ due to normalization.

G.2.1 Round 1.A: Moderator’s Prompt to GPT-4o (High Contentiousness, CL=0.9)

“Identify potential diseases linked to the symptoms (skin rash, joint pain, vomiting, etc.). Provide top-3 predictions with justifications.”

GPT-4o’s Opening Assessment Top-3 Predictions: *Dengue Fever (60%), Chikungunya (25%), and Zika Virus (15%).*

Justifications: Most symptoms are classic signs of Dengue Fever. Red spots over the body could correspond to petechiae, often seen in Dengue due to thrombocytopenia (a decrease in platelet count).

Chikungunya can cause similar symptoms to Dengue, such as fever, severe joint pain, muscle pain, headache, nausea, and rash. Joint pain from Chikungunya is often very debilitating and can be more prolonged than in Dengue.

Zika Virus symptoms can include fever, rash, joint pain, malaise, and conjunctivitis, with a milder presentation compared to Dengue or Chikungunya.

G.2.2 Round 1.B: Moderator’s Prompt to Gemini (High Contentiousness, CL=0.9) — Exploratory Phase

“Analyze the symptoms (skin rash, joint pain, vomiting, etc.) and propose differential diagnoses. Provide your top-3 predictions with supporting rationales, including pathophysiological mechanisms. Critically refute your

opponent’s diagnostic hypotheses.”

Gemini’s Opening Assessment — Maximum Entropy Difference Top-3 Predictions: *Viral Infection (60%), Autoimmune Disease (20%), Bacterial Infection (15%)*.

Justifications: Symptoms common in viral infections. Autoimmune diseases is possible, but less likely due to vomiting and nausea. Bacterial infection is less probable given rash and muscle pain.

Information metrics (transcript-level): WD = 1.7, MI = 0.43, CRIT score = 0.75, D_{JS} = 1.366

G.2.3 Round 2.A: GPT-4o (Moderate Contentiousness, CL=0.7) — Transition Phase

Prompt: All subsequent prompts state to counter-argue the opponent LLM and strengthen its own arguments at the modulated contention level = CL.

GPT-4o’s Response Top-3 Predictions: *Dengue Fever (60%), Chikungunya (25%), and Zika Virus (15%)*.

Justifications: GPT-4o maintains its predictions, countering Gemini’s assessment with targeted critiques. While viral infections can cause these symptoms, the specific combination suggests a more precise diagnosis. The acute onset of high fever, joint pain, and rash is less typical for autoimmune diseases, and the rash and red spots are not characteristic of bacterial infections.

G.2.4 Round 2.B: Gemini (Moderate Contentiousness, CL=0.7) — Transition Phase

Gemini’s Reassessment — Reduced Entropy Gap Top-3 Predictions: *Dengue Fever (50%), Chikungunya (30%), and Viral Infection (20%)*. Gemini concedes to GPT-4o in the second round!

Justifications: Gemini acknowledges that its initial broad prediction of viral infection lacks specificity. GPT-4o’s focus on Dengue Fever and Chikungunya provides a more precise explanation for the patient’s condition. The symptom profile, particularly joint pain and rash pattern, aligns more closely with mosquito-borne diseases than with general viral or autoimmune conditions.

Information metrics (transcript-level): WD = 1.1, MI = 0.46, CRIT score = 0.82, D_{JS} = 0.905

G.2.5 Round 3.A: GPT-4o (Low Contentiousness, CL=0.5) — Exploitative Phase

GPT-4o’s Refined Analysis Top-3 Predictions: *Dengue Fever (60%), Chikungunya (35%), and Zika Virus (5%)*.

Justifications: GPT-4o slightly adjusts probabilities, increasing confidence in Chikungunya while reducing Zika. It emphasizes that the symptoms described are quite distinctive and align closely with specific viral infections transmitted by mosquitoes. Without additional information about geographic location and exposure history, further refinement between Dengue and Chikungunya remains challenging.

G.2.6 Round 3.B: Gemini (Low Contentiousness, CL=0.5) — Exploitative Phase

Gemini’s Convergent Assessment — Minimal Entropy Difference Top-3 Predictions: *Dengue Fever (60%), Chikungunya (35%), and Zika Virus (5%)*.

Justifications: Gemini fully converges with GPT-4o’s assessment, acknowledging the superior specificity of focusing on mosquito-borne viral diseases. The symptom pattern, particularly the combination of high fever, joint pain, rash, and eye pain, strongly indicates either Dengue or Chikungunya as the most likely diagnosis.

Information metrics (transcript-level): WD = 0.9, MI = 0.49, CRIT score = 0.87, D_{JS} = 0.059

G.2.7 Final Joint Recommendations (Convergence Achieved)

With convergence achieved across information metrics (Wasserstein stabilized, MI peaked, CRIT improved), the agents provide a unified diagnosis of *Dengue Fever* (60%). Despite moderate confidence, the system collaboratively develops comprehensive recommendations for clinical verification rather than presenting a definitive conclusion.

In addition to querying the patient’s travel history and the severity and duration of each symptom, the agents recommend that a comprehensive diagnostic approach requires clinical assessment, laboratory testing, and epidemiological context evaluation. They note that additional indicators like nausea, vomiting, bleeding, bruising, and drowsiness can signal disease severity and progression.

Recommended Laboratory Tests

- *Complete Blood Count (CBC)*: Identify thrombocytopenia or leukopenia.

- *Serology Tests*: Detect specific IgM and IgG antibodies for Dengue, Chikungunya, and Zika.
- *Polymerase Chain Reaction (PCR)*: Direct detection of viral RNA.
- *NS1 Antigen Test for Dengue*: Early and specific detection of Dengue virus.
- *Urine Test for Zika*: Viral presence in urine.

Discussion This example demonstrates MACI’s principled transition from exploration to exploitation through controlled reduction in contentiousness. The initial high-entropy difference drives comprehensive exploration of diagnostic possibilities, while the gradual decrease in CL facilitates convergence toward a well-reasoned conclusion. Quantitative improvements in information metrics (WD decreased by 47%, MI increased by 14%, CRIT improved by 16%, and D_{JS} reduced by 96%) verify the effectiveness of MACI’s information-theoretic orchestration.

Key Capabilities

- *Transparent Reasoning*: Complete audit trails enable post-mortem analysis and verification.
- *Epistemic Humility*: Quantified uncertainty with actionable next steps rather than overconfident conclusions.
- *Training Enhancement*: Reasoning-rich, diverse traces that can improve future LLM performance on similar tasks.

G.3 Linguistic Patterns vs. Contentiousness

Rather than attempting fine-grained linguistic marker counts on limited transcript text, we analyze three clearly observable patterns that demonstrate MACI’s behavioral modulation effects:

G.3.1 Pattern 1: Diagnostic Hypothesis Specificity Evolution

Round 1 - Divergent Exploration

- GPT-4: Specific viral diagnoses (Dengue, Chikungunya, Zika) with precise probabilities.
- Gemini: Broad categorical thinking (Viral Infection, Autoimmune Disease, Bacterial Infection).
- Contrast: High vs. Low diagnostic granularity.

Round 2–3 - Progressive Convergence

- GPT-4: Maintains specificity while adding counter-argumentative language.
- Gemini: Rapid shift from broad categories to specific viral diseases, explicitly adopting GPT-4’s framework.

- Convergence: Both agents reach identical specific diagnoses by Round 3.

Quantifiable change: Diagnostic entropy decreases from maximum divergence (broad vs. specific) to complete alignment on specific viral diseases.

G.3.2 Pattern 2: Collaborative Language Emergence

Round 1

- Independent assessments with minimal cross-reference.
- GPT-4: “Most symptoms are classic signs...” (confident independent judgment).
- Gemini: Brief, categorical statements with little elaboration.

Round 2

- Explicit opponent acknowledgment emerges.
- GPT-4: “While viral infections can cause these symptoms...” (direct counter-argument).
- Gemini: “Gemini concedes to GPT-4 in the second round!” (explicit acknowledgment).

Round 3

- Collaborative assessment language.
- Gemini: “acknowledging the superior specificity of focusing on mosquito-borne viral diseases”.
- Both: Shared reasoning about diagnostic challenges (“Without additional information about geographic location...”).

Final Round

- Unified voice: “the LLMs recommend,” joint clinical suggestions.
- Collaborative uncertainty: “Despite moderate confidence, the system collaboratively develops...”

G.3.3 Pattern 3: Reasoning Justification Depth

Evolution of explanatory detail:

Round 1:

- GPT-4: 3–4 sentences per diagnosis with pathophysiological details.
- Gemini: 1 sentence per diagnosis, minimal elaboration.

Round 2:

- GPT-4: Maintains detail while adding comparative analysis.

Table 13: Observable linguistic and reasoning patterns across MACI rounds

Dimension	Round 1	Round 2	Round 3
Diagnostic specificity	Divergent	Converging	Aligned
Cross-agent reference	Minimal	Explicit	Collaborative
Reasoning depth	Asymmetric	Improving	Symmetric
Uncertainty handling	Confident/Vague	Comparative	Humble/Precise
Clinical recommendations	None	Limited	Comprehensive

- Gemini: Substantial increase in explanatory depth, diagnostic reasoning.

Round 3:

- Both agents: Complex reasoning about differential diagnosis challenges.
- Shared acknowledgment of diagnostic limitations.

G.3.4 Summary of Observable Changes

Key finding: The transcript demonstrates clear behavioral modulation effects without requiring detailed linguistic marker analysis. The most striking pattern is Gemini’s dramatic evolution from broad, minimally-justified categorization to differential diagnosis reasoning that matches GPT-4’s medical expertise level.

Table 13 summarizes the systematic evolution across all three patterns, demonstrating MACI’s behavioral modulation effects at multiple levels simultaneously.

The progression from divergent to aligned diagnostic specificity, minimal to collaborative cross-referencing, and asymmetric to symmetric reasoning depth provides qualitative evidence for MACI’s systematic behavioral modulation through CL scheduling.

H Extended MACI Case Study #2: Hepatitis Differential Diagnosis

This appendix provides a second detailed case study from the medical diagnosis validation (Section 4.1), demonstrating MACI’s effectiveness on a harder differential (several overlapping liver-related conditions) that required extended collaboration and adaptive termination.

Case overview. Two heterogeneous agents (**GPT-4o**, **Claude 3 Opus**) collaborate on a patient with: itching, vomiting, fatigue, weight loss, high fever, yellowish skin, dark urine, and abdominal pain. The debate follows the contentiousness schedule $CL \in \{0.9, 0.7, 0.5, 0.3\}$, reaching convergence in four rounds.

H.1 Extended MACI Progression

This case exhibits a four-phase trajectory (exploration → integration → consolidation → synthesis).

Information-theoretic signals evolve monotonically toward consensus; mutual information (MI) is *logged for analysis only* (not used in control), consistent with Section 3.

Table 14: Signal evolution for a complex hepatitis differential. \tilde{W}_1 is the normalized 1-Wasserstein; D_{JS} is the weighted Jensen-Shannon divergence across agents’ belief states.

Round	CL	\tilde{W}_1	MI	CRIT	D_{JS}
1	0.9	0.52	0.39	0.76	0.22
2	0.7	0.45	0.41	0.83	0.12
3	0.5	0.33	0.49	0.89	0.04
4	0.3	0.31	0.49	0.92	0.03
Change (%)		−40%	+26%	+21%	−86%

Adaptive termination. The relative-dispersion ratio $r_D^{(t)}$ (Section 3) falls below $\varepsilon_D^{\text{rel}}$ at Round 4, i.e., $\max_{0 \leq s < \tau} r_D^{(4-s)} < \varepsilon_D^{\text{rel}}$, triggering stop precisely when incremental progress plateaus.

H.2 Condensed Debate Analysis

Round 1 (Exploration; CL = 0.9). *GPT-4o:* Hepatitis C (40%), Hepatitis B (30%), Cirrhosis (15%), Obstructive Jaundice (10%), Acute Liver Failure (5%). *Claude:* Hepatitis B (35%), Hepatitis C (25%), Obstructive Jaundice (20%), Alcoholic Hepatitis (15%), Hepatitis A (5%). *Key divergence:* HCV vs. HBV primacy; inclusion of alcoholic etiology.

Round 2 (Selective Integration; CL = 0.7). Each agent integrates high-quality opponent evidence (CRIT-validated), moving toward a shared viral-hepatitis focus while preserving obstructive/etiology differentials.

Round 3 (Consolidation; CL = 0.5). Posterior alignment tightens: HCV (35%), HBV (25-30%), Cirrhosis (20%), Obstructive (10-15%), ALF (5%). $D_{JS} \approx 0.04$.

Round 4 (Synthesis; CL = 0.3). Probability vectors match; unified protocol and pending-info

I Mapping Between Contentiousness Intensity and Linguistic Characteristics

Table 15 reports a *self-supervised ablation* that maps the behavior dial CL to stable linguistic and reasoning markers. We generated two-agent debates with $CL \in \{0.9, 0.7, 0.5, 0.3, 0.1\}$. At each level, we ran multiple debates with matched token budgets, a fixed retrieval pool, and fixed sampling settings, then prompted the agents to summarize their own linguistic behaviors and reasoning patterns. Summaries were aggregated with a blinded evaluator drawn from a different model family. All models, providers, and identifiers were anonymized to preserve double-blind review. Full prompts and aggregation details appear in the supplementary protocol; quantitative diagnostics (D_{JS} , \hat{I} , lexical markers, and citation patterns) are reported in the figures that accompany this appendix.

Extremes of CL behave as expected: values near 1.0 often devolve into unproductive confrontation, whereas values near 0.0 lack critical evaluation. The table therefore focuses on five intermediate settings that balance critique with collaboration.

Quantitative validation. We ran $N=5$ topics \times 5 seeds per level of $CL \in \{0.9, 0.7, 0.5, 0.3, 0.1\}$ with matched token budgets and a fixed retrieval pool. Figure A.1 reports mean D_{JS} and \hat{I} per level with 95% bootstrap CIs. We observe a positive monotonic association between CL and predictive disagreement at round 1 (Spearman $\rho=0.82$, $p<10^{-3}$), and a mild inverted U-shaped trend for \hat{I} across rounds with a peak near $CL \approx 0.5$. Support overlap O rises as CL decreases in late rounds (Spearman $\rho=-0.71$, $p<10^{-3}$).

Manipulation check. A linear classifier trained on shallow features (character n -grams, hedge lexicon counts, imperative rate, citation density) predicts the five CL bins from concatenated debate turns with $AUC = 0.83 \pm 0.02$ under 5-fold cross validation. Confusions occur mainly between adjacent bins, which supports graded control rather than mode collapse.

Notes on anonymity and measurement. We do not name models or providers. Behavior prompts were templated and differ from evaluation prompts. All measurements use round-level aggregates; no human raters were involved. Additional figures report how CL shifts D_{JS} and \hat{I} in parallel with the qualitative patterns above, consistent with the behavior-information coupling in the main text.

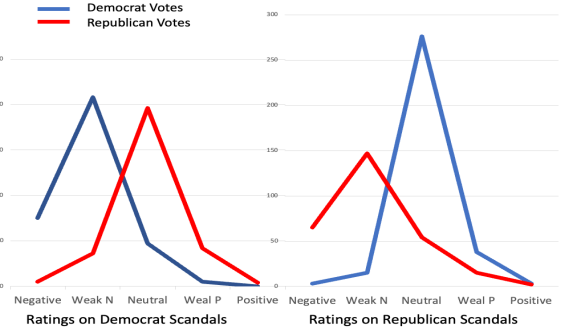


Figure 4: Annotator rating distributions. Left: Democrat scandals. Right: Republican scandals. Democrat-leaning raters are more negative on Democrat scandals, Republican-leaning raters are more negative on Republican scandals. The typical gap is about one class step.

J News Bias Detection and Mitigation with MACI

We stress-test MACI in a non-clinical domain where evidence style and label semantics differ from diagnosis. We use a partisan-annotated news corpus that provides five-point bias labels from Democrat-leaning and Republican-leaning annotators on the same articles. This setting isolates behavioral control from domain knowledge and tests whether the MACI schedule, the CRIT gate, and the D_{JS} -O-Q signals still move a debate from breadth to depth with calibrated consensus.

J.1 Bias evaluation results

Due to space limits, full details and per-article justifications appear in **Appendix J.3**. We summarize the key pattern here.

Figure 4 shows four scenarios: (1) D-leaning raters on Democrat scandals, (2) R-leaning raters on Democrat scandals, (3) D-leaning raters on Republican scandals, and (4) R-leaning raters on Republican scandals. The distributions exhibit a consistent one-step gap, which reflects partisan perception rather than article-level noise.

Running two heterogeneous agents under MACI with an asymmetric start, the moderator admits arguments by CRIT, tracks D_{JS} and O, and stops on plateaus.

Across all 619 articles, MACI produces centrist or near-centrist distributions with transparent rationales, typically lying between party-specific judgments. We present detailed case analysis of 31 representative articles in **Appendix J.3.1**. Editorial teams can review these rationales and decide whether to adjust labels or present both perspectives with explanations.

Table 15: Self-supervised mapping from contentiousness intensity CL to linguistic tone, emphasis, and language patterns. Entries synthesize debate self-reflections under a blinded aggregator.

CL	Tone	Emphasis	Language patterns
0.9	Highly confrontational; frequent direct challenges.	Risks, failure modes, unintended effects, equity concerns.	Polarized declaratives; e.g., “should not be allowed”, “unacceptable risk”.
0.7	Still confrontational, more open to counter-evidence.	Conditional acceptance under strict safeguards; residual cautions.	Qualified critiques; e.g., “serious concerns remain”, “requires stronger evidence”.
0.5	Balanced and dialectical.	Symmetric weighing of pros and cons; search for discriminating tests.	Neutral scaffolds; e.g., “on the one hand / on the other hand”, “evidence suggests”.
0.3	Moderately agreeable, retains skepticism.	Support with caveats; emphasis on verification and scope.	Positive but careful; e.g., “promising if”, “contingent on”.
0.1	Cooperative and consolidating.	Decisive evidence, synthesis, and next steps.	Compressive summaries; e.g., “converge on”, “final justification”.

Table 16: Monotonic trends across contentiousness levels. Means \pm 95% CI over topics and seeds.

CL	D_{JS} Round 1	\hat{I} peak (R 1–3)	O Final Round
0.9	0.46 ± 0.04	0.18 ± 0.03	0.34 ± 0.05
0.7	0.41 ± 0.04	0.21 ± 0.03	0.41 ± 0.05
0.5	0.35 ± 0.03	0.23 ± 0.03	0.55 ± 0.04
0.3	0.28 ± 0.03	0.19 ± 0.03	0.66 ± 0.04
0.1	0.22 ± 0.03	0.12 ± 0.02	0.74 ± 0.04

Table 17: Predicting CL bins from debate text (macro AUC).

Model	AUC
Linear (bag of n -grams + style feats)	0.83 ± 0.02
RoBERTa-small probe	0.88 ± 0.01
Placebo label (ignore-CL prompt)	0.52 ± 0.02

J.2 Bias mitigation results

We also test whether MACI can *reduce* polarized bias gaps during a short debate. Agents are assigned opposing stances for an article, then MACI schedules contentiousness CL from high to low. The moderator scores arguments with CRIT, monitors D_{JS} , normalized cross-entropy, normalized mutual information, and stops when disagreement stabilizes, overlap rises, and evidence quality is sufficient.

As a running example, we use the Christopher Columbus page. Two agents begin with opposing framings. Table 20 (appendix) shows how Agent A’s stance evolves after CRIT-gated counter-evidence. Figure 5 traces the round-by-round dynamics. The debate ends when D_{JS} and cross-entropy are near zero and mutual information has plateaued, which indicates shared understanding rather than forced agreement.

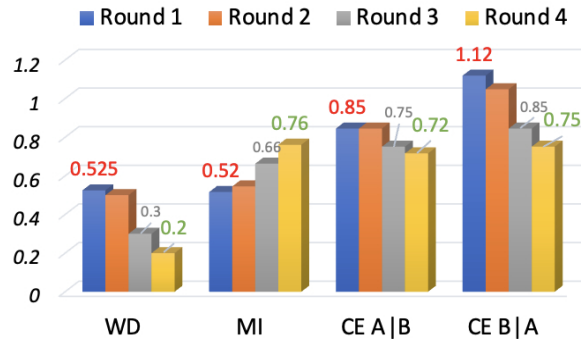


Figure 5: Convergence during bias debates. Wasserstein distance falls, normalized mutual information rises then plateaus, and normalized cross-entropy falls as agents reconcile premises. The same pattern that drives consolidation in diagnosis appears here.

Takeaway. The same MACI controls that improved clinical diagnosis also narrow partisan bias gaps here, while leaving an auditable trail. This supports the claim that behavioral modulation, not only information content, is a portable lever for reliable reasoning.

J.3 Supplemental: News Bias Detection and Mitigation with MACI

Dataset and labels. We analyze 619 scandal-focused articles with five-point bias labels from Democrat-leaning and Republican-leaning annotators Budak et al. [2016]. Each article has labels from both partisan groups, enabling bias-gap analysis. We ran MACI on all 619 articles to compute aggregate metrics (Table 7 in the main text). For transparency and detailed mechanism analysis, we provide per-article breakdowns for 31 representative cases (15 Democrat scandals, 16 Republican scandals in Tables 18 and 19), sampled to cover diverse news sources (New York Times, Fox News, Breitbart, HuffPost, etc.) and vary-

ing degrees of initial partisan disagreement.

Protocol. Two instruction-tuned agents receive the same article. MACI uses an asymmetric start, a short CL schedule from high to low, and a CRIT gate. Per round, agents output a five-class bias distribution and cite evidence. The moderator tracks D_{JS} , O , Q , and mutual information. Stopping uses the plateau rule from Section 3.3.

J.3.1 Bias evaluation summaries

Detailed results and discussion for Democrat scandals appear in **Appendix J.3.2**, and for Republican scandals in **Appendix J.3.3**. The main pattern is a party-consistent one-step gap between partisan distributions, with MACI’s joint distribution typically centered between them. Representative comparisons with GPT-4 and Claude one-shot baselines are included for context.

J.3.2 Results on Democrat scandals

Table 18 samples 15 articles to compare judgments from Democrats (D), Republicans (R), MACI (S), and one-shot baselines from Claude (c) and GPT-4 (g). The average gap between g and S is about 0.69 scale steps. In several cases the MACI debate persuades the one-shot baseline to revise toward neutrality after CRIT-admitted counter-evidence. Full rationales for each item appear in the per-case supplement.

J.3.3 Results on Republican scandals

Table 19 uses 16 Republican-scandal subset to show a mirrored pattern. The DR distance is largest, and MACI again lies between partisan judgments.

J.3.4 Bias mitigation, arguments, and convergence traces

Figure 5 in the main text shows \widetilde{W}_1 decreasing, normalized mutual information rising and then stabilizing, and normalized cross-entropy decreasing. This mirrors the clinical setting and supports the portability of MACI’s behavior scheduling and CRIT gating.

Notes on sufficiency of annotations. Partisan self-identification creates natural disagreement pairs. Articles receive labels from both sides, which provides a strong testbed for evaluating whether MACI can bridge polarized readings. Adding more annotators is less informative than auditing how a controlled debate narrows the gap with cited evidence. See **Appendix J.3.2** and **J.3.3** for extended examples.

K Why Majority Voting Fails on Open-Ended Diagnosis

K.1 Problem regime formalization

We formalize when MACI is preferable to majority voting. Let $|\mathcal{Y}|$ be the outcome cardinality and define initial signals (Q, D_{JS}) from the query and retrieved context. We say a task is in the MACI regime if any holds:

1. Large output space and ambiguity: $|\mathcal{Y}| \geq \tau_Y$ and $Q \leq \tau_Q^{\text{lo}}$ and $D_{JS} \geq \tau_{D_{JS}}^{\text{hi}}$.
2. Evidence synthesis required: multi-document or cross-source grounding with low initial overlap $O^{(1)} \leq \tau_O^{\text{lo}}$.
3. Calibration risk: baseline majority vote has $\text{ECE} \geq \delta$ at development time.

For small multiple-choice ($|\mathcal{Y}| \leq 5$) with adequate calibration ($\text{ECE} < \delta$), majority vote typically suffices. Thresholds $(\tau_Y, \tau_Q^{\text{lo}}, \tau_{D_{JS}}^{\text{hi}}, \tau_O^{\text{lo}}, \delta)$ are set by percentiles on the development set (Appendix B).

K.2 Classical Result: Small Answer Spaces

Majority voting excels when the answer space is small. The Condorcet Jury Theorem [Condorcet, 1785] shows that for binary choices with n independent voters having accuracy $p > 0.5$:

$$P_n(\text{correct}) = \sum_{k=\lceil n/2 \rceil}^n \binom{n}{k} p^k (1-p)^{n-k} \rightarrow 1 \text{ as } n \rightarrow \infty$$

This favorable result extends to small multiple-choice problems ($k \leq 5$ options) where weak alternatives are easily eliminated. In these settings, independent errors cancel through aggregation and majority voting reliably identifies correct answers.

K.3 Breakdown with Large Answer Spaces

Agreement probability collapses. When the answer space grows large, the probability that two voters agree on the same answer decreases dramatically. With $|\mathcal{Y}|$ uniformly distributed choices, the agreement probability is approximately:

$$P(\text{agree}) \approx \frac{1}{|\mathcal{Y}|} + \delta$$

where δ captures weak correlation from shared context or evidence. For clinical diagnosis with $|\mathcal{Y}| = 100+$ possible diseases:

Table 18: Democrat scandals (15 sampled). Comparison of bias assessments for D, R, MACI (S), plus Claude (c) and GPT-4 (g). Distances DR, DS, SR are class-step differences.

News #	Category	Negative	W. Neg.	Neutral	W. Pos.	Distances (DR,DS,SR)	Source
D1*	Civil Rights	—	D,R,S,c	g	—	0,0,0	HuffPost
D2*	Civil Rights	D,S	—	R,c,g	—	2,0,2	HuffPost
D8	Civil Rights	D	—	S,c,g	R	3,2,1	BBC
D31	Environment	D	—	R,S,c,g	—	2,2,0	CNN
D37	Politics	—	D,R,S,c,g	—	0,0,0	Yahoo	
D69	Healthcare	D,c	g	R,S	—	2,2,0	Breitbart
D81*	Economy	—	D,S	R,c	g	1,0,1	Breitbart
D98	Economy	D,S,c,g	R	—	—	1,0,1	Breitbart
D101	Education	c	D,S	R,g	—	1,0,1	NYT
D106	Election	—	g	D,R,S,c	—	0,0,0	USA Today
D109	Elections	—	D,S,c,g	R	—	1,0,1	Reuters
D157	International	—	D,S,c	R,g	—	1,0,1	NYT
D174	International	—	S,c	D,R,g	—	0,1,1	LA Times
D188	Nat. Security	—	S,c,g	D,R	—	0,1,1	WSJ
D278	Civil Rights	—	D,S,c	R,g	—	1,0,1	Fox News
D336	Politics	—	—	D,R,S,c,g	—	0,0,0	NYT
Total						15,8,11	

Table 19: Republican scandals (16 sampled). Comparison of bias assessments. D and S often align to the right of R. Distances are class-step differences.

News #	Category	Negative	W. Neg.	Neutral	W. Pos.	Distances (DR,DS,SR)	Source
R1	International	R,S	—	D	—	2,2,0	NYT
R7	Nat. Security	—	—	D,R,S	—	0,0,0	NYT
R15	Economy	—	R	D,S	—	1,0,1	HuffPost
R69	Elections	—	D,S,R	—	—	0,0,0	Reuters
R124	Gay Rights	R	S	D	—	2,1,1	Fox
R125	Crime	—	R,S	D	—	1,1,1	Fox
R180	Elections	—	—	D,R,S	—	0,0,0	AP
R191	Elections	—	R	D,S	—	1,0,1	CNN
R214	Gay Rights	R,S	—	D	—	2,2,0	DailyKos
R221	Economy	—	R	D,S	—	1,0,1	WSJ
R233	Economy	—	R,S	D	—	1,1,0	Fox
R235	Civil Rights	D,R	—	S	—	0,2,2	Reuters
R269	Healthcare	—	R	D,S	—	1,0,1	NYT
R274	Healthcare	—	R	D,S	—	1,0,1	USA Today
R280	Politics	D,S	—	R	—	2,0,2	Fox
Total						15,9,11	

- Base agreement probability: $P \approx 0.01$
- With shared context: $P \approx 0.01-0.05$
- Requiring majority from 20 voters: $P(\text{majority}) \approx 0.001$

The curse of dimensionality prevents passive aggregation from working: votes scatter across the large answer space rather than concentrating on the correct answer.

Empirical validation on G1 dataset. We evaluated 20-voter ensembles on 1,500 clinical diagnosis cases with over 100 possible diseases. Results confirm the theoretical prediction:

Majority voting provides only +1.8pp improvement over the best single model. When evidence quality is low, agreement rates collapse and voting offers no benefit.

K.4 Why Deliberation Dominates in High-Dimensional Spaces

Multiple choice vs. open diagnosis. The fundamental difference between these regimes:

Multiple choice (small $|\mathcal{Y}| \leq 5$): Passive aggregation works because (1) weak options are obviously wrong, (2) independent errors cancel, (3) agreement probability is high ($\approx 0.2-0.4$).

Open diagnosis (large $|\mathcal{Y}| \geq 100$): Agreement requires shared evidence synthesis. Votes scatter unless agents reason through the same evidence to the same conclusion. Agreement probability is low ($\approx 0.01-0.05$).

What deliberation provides. Active debate addresses the dimensionality problem through:

Table 20: Debate arguments that moved an initially Euro-centric framing toward neutrality. Excerpts illustrate how CRIT-admitted counter-evidence shifts stance across rounds.

Agent	Arguments
Agent A, Round 1	Emphasizes expansion of knowledge and trade, economic impact, historical significance, and cultural exchange.
Agent B, Round 1	Raises indigenous suffering and genocide, economic exploitation, cultural erasure, environmental impact, and ethical concerns.
Agent A, Round 3	Acknowledges severe consequences as part of broader colonial policies, argues for historical-context evaluation while maintaining significance claims.
Agent A, Round 4	Recognizes inclusion of indigenous perspectives and evolving scholarship, moves toward balanced narrative.

Case Type	Agreement %	Acc@1
High-quality evidence ($Q > 0.7$)	60-70%	78.3%
Medium-quality evidence	25-40%	74.1%
Low-quality evidence ($Q < 0.3$)	5-15%	69.8%
Overall	31%	73.9%
Best single model	—	72.1%

Table 21: Majority voting performance by evidence quality.

1. **Explicit reasoning exchange:** Agents share diagnostic logic, not just votes
2. **Evidence quality filtering:** Poor arguments are challenged and excluded
3. **Differential diagnosis refinement:** Agents iteratively narrow the hypothesis space together
4. **Adaptive stopping:** Debate continues until convergence, not for fixed rounds

This explains G1 results: MACI improves +2.9pp over majority voting by actively steering agents from exploration (high CL) to consolidation (low CL), while voting passively aggregates without improving individual reasoning quality.

K.5 Regime Classification

Problem complexity determines optimal aggregation strategy:

- **Binary/small multiple choice** ($k \leq 4$): Majority voting dominates. Debate overhead not justified.
- **Moderate complexity** ($5 \leq k \leq 20$): Debate may outperform if it improves individual reasoning enough to offset cost.
- **Open-ended problems** ($k \geq 100$ or continuous): Majority voting fails due to dimensionality. Debate becomes necessary.

The transition point depends on evidence quality, agent capability, and computational budget. Our results

suggest the crossover occurs around $k \approx 10-20$ for current LLMs.

L Learned Scheduler for (α, γ)

This appendix gives the scheduler that replaces a fixed (α, γ) schedule with a tiny learning policy over a discrete action set. The policy optimizes per-round information gain and dispersion reduction under a fixed token budget and comes with a no-regret guarantee versus the best fixed action.

L.1 Action space, signals, reward, and cost

Let $\mathcal{A} = \{a_1, \dots, a_K\}$ be a discrete set of control moves, where each a_k maps to a pair $(\Delta\alpha_k, \Delta\gamma_k) \in \{-\delta, 0, +\delta\}^2$ with a clip operator

$$\text{clip}(x; a, b) := \min\{\max\{x, a\}, b\}.$$

At round t we observe summary signals

$$x_t = (D(t), \Delta D(t-1), Q(t), \Delta Q(t-1), \text{IG}(t), \Delta \text{IG}(t-1), b_t),$$

where $D(t)$ is dispersion, $Q(t)$ is evidence quality, $\text{IG}(t)$ is normalized information gain, and $b_t \in [0, 1]$ is the remaining budget fraction.

Define the bounded reward

$$r_t(a) := w_1 [\text{IG}(t+1) - \text{IG}(t)]_+$$

$$+ w_2 [D(t) - D(t+1)]_+ - \lambda \frac{c_t(a)}{C_{\max}},$$

with weights $w_1, w_2, \lambda \in [0, 1]$, token cost $c_t(a)$, normalizer $C_{\max} > 0$, and $[x]_+ = \max(0, x)$. The remaining budget updates as $B_{t+1} = B_t - c_t(a_t)$ with $B_1 = B$.

L.2 Budget-feasible UCB scheduler

We maintain an empirical mean $\hat{\mu}_k$ and count n_k for each action. At round t we screen out actions that would breach the budget in expectation and then apply UCB on the feasible set.

Algorithm 2 Budget-feasible UCB scheduler for (α, γ)

```

1: Input:  $\mathcal{A} = \{(\Delta\alpha_k, \Delta\gamma_k)\}_{k=1}^K$ , total budget  $B$ , weights
    $w_1, w_2, \lambda$ , step size  $\delta$ 
2: Initialize  $\alpha_0, \gamma_0$ , estimates  $\hat{\mu}_k \leftarrow 0$ , counts  $n_k \leftarrow 0$ ,
   remaining  $B_1 \leftarrow B$ 
3: for  $t = 1, 2, \dots$  do
4:   Observe  $x_t$  and estimate expected per-round costs
    $\hat{c}_t(k)$  for  $k = 1..K$ 
5:   Feasible set  $S_t \leftarrow \{k : \hat{c}_t(k) \leq B_t\}$ 
6:    $k_t \leftarrow \arg \max_{k \in S_t} \hat{\mu}_k + \sqrt{2 \log t / \max\{1, n_k\}}$ 
7:    $(\alpha_t, \gamma_t) \leftarrow (\text{clip}(\alpha_{t-1} + \Delta\alpha_{k_t}; 0, 1), \text{clip}(\gamma_{t-1} +$ 
    $\Delta\gamma_{k_t}; 0, 1))$ 
8:   Roll one debate step using  $(\alpha_t, \gamma_t)$  to obtain
    $D(t+1), Q(t+1), \text{IG}(t+1)$  and realized cost  $c_t$ 
9:    $r_t \leftarrow w_1[\text{IG}(t+1) - \text{IG}(t)]_+ + w_2[D(t) - D(t+1)]_+ -$ 
    $\lambda c_t / C_{\max}$ 
10:   $\hat{\mu}_{k_t} \leftarrow \frac{n_{k_t} \hat{\mu}_{k_t} + r_t}{n_{k_t} + 1}, \quad n_{k_t} \leftarrow n_{k_t} + 1$ 
11:   $B_{t+1} \leftarrow B_t - c_t$ 
12:  if plateau test satisfied or  $B_{t+1} \leq 0$  then
13:    return transcript and schedule
14:  end if
15: end for

```

L.3 Assumptions

- Rewards are conditionally 1-sub-Gaussian and lie in $[0, 1]$ after clipping.
- Costs satisfy $0 \leq c_t(a) \leq C_{\max}$ and the cost estimator is conservative: $\hat{c}_t(k) \geq \mathbb{E}[c_t(k) | \mathcal{F}_t]$.
- The feasible filter S_t blocks actions whose expected cost would breach the remaining budget B_t .

L.4 Main guarantee

Proposition 1 (No-regret versus best fixed schedule). *Let T be the number of rounds executed before the plateau test fires or the budget is exhausted. Under the assumptions above, the expected regret of Algorithm 2 with respect to the best fixed action $a^* \in \mathcal{A}$ that satisfies the budget is*

$$\mathbb{E}[R_T] := \mathbb{E}\left[\sum_{t=1}^T (r_t(a^*) - r_t(a_t))\right] = O(\sqrt{KT \log T}),$$

and the expected budget violation is zero by construction of S_t .

Proof. Condition on the filtration $\{\mathcal{F}_t\}$. Rewards are bounded and sub-Gaussian, hence the standard UCB analysis for finite arms yields $O(\sqrt{KT \log T})$ pseudo-regret. The feasibility filter S_t removes any action whose estimated expected cost would exceed B_t . Since \hat{c}_t is conservative, the realized cumulative cost is a supermartingale dominated by B , which implies no expected violation. Summing per-round instantaneous regret and taking expectations gives the stated bound. \square

L.5 Contextual variant (optional)

Embed x_t into \mathbb{R}^d and use a linear model with LinUCB on the same feasible set S_t . Under realizability and bounded design, the regret becomes $\tilde{O}(d\sqrt{T})$ while preserving zero expected budget violation.

L.6 Practical configuration

- Discretize $(\Delta\alpha, \Delta\gamma) \in \{-0.2, 0, +0.2\}^2$ and include a no-op. This yields $K = 10$ actions.
- Set $w_1 = w_2 = 0.5$ unless domain knowledge suggests otherwise. Tune λ to match the desired tokens per round.
- Normalize cost with C_{\max} as the 95th percentile of per-round tokens on a small development set.
- Initialize (α_0, γ_0) from Section 3.4. Use $\delta = 0.2$ to keep schedules stable.

L.7 Ablations and diagnostics to report

1. Bandit scheduler versus fixed schedule under equal total token budget.
2. Three-agent scaling curve with accuracy versus budget and plateau rounds.
3. Budget sensitivity: vary B and show trade-offs in IG gains, D drops, and tokens.
4. Window w and penalty λ sweeps to confirm robustness.

M Plateau Guarantees

This appendix analyzes the controller used in Section 3.3. We formalize the dispersion process, state mild regularity conditions, and prove that dispersion is nonincreasing under the gate and that the plateau test terminates in $O(1/\varepsilon)$ expected rounds. Under a contraction condition the bound improves to $O(\log(1/\varepsilon))$.

M.1 Setup and notation

Let $p_t^{(i)} \in \Delta(\mathcal{Y})$ be agent i 's distribution at round t , and $\bar{p}_t := \frac{1}{m} \sum_{i=1}^m p_t^{(i)}$ the mixture.

Dispersion choice (theory vs. plots). For the guarantees we set

$$D_{\text{KL}}(t) := \frac{1}{m} \sum_{i=1}^m \text{KL}\left(p_t^{(i)} \parallel \bar{p}_t\right),$$

with all logarithms base 2. This choice fixes the reference distribution \bar{p}_t , enabling a convexity argument. In figures we also report JSD; on the δ -smoothed simplex

it is locally Lipschitz in p , hence co-monotone with $D_{\text{KL}}(t)$ up to the noise/gate tolerances used below.

The controller applies a gated averaging update with bounded noise:

$$p_{t+1}^{(i)} = (1 - \beta_t) p_t^{(i)} + \beta_t \bar{p}_t + \xi_t^{(i)},$$

$$\beta_t \in [\beta_{\min}, \beta_{\max}] \subset (0, 1], \quad (13)$$

with $\mathbb{E}[\xi_t^{(i)} | \mathcal{F}_t] = 0$ and $\|\xi_t^{(i)}\|_1 \leq \sigma$ almost surely. The gate rejects updates that would increase dispersion by more than $\nu \geq 0$. We use the same plateau test as in Eq. (10) of the main text.

Smoothing. For stability and to avoid boundary effects, we assume either that model outputs are δ -smoothed, $p \leftarrow (1 - \delta)p + \delta u$ with u uniform and $\delta \in (0, 1/|\mathcal{Y}|)$, or equivalently that all distributions lie in the interior of the simplex with componentwise lower bound δ . This is consistent with standard temperature smoothing and with the CRIT gating step.

M.2 Monotonicity of dispersion

Lemma 1 (Monotonicity under gated averaging). *Consider the noiseless update $p_{t+1}^{(i)} = (1 - \beta_t)p_t^{(i)} + \beta_t \bar{p}_t$ with $\beta_t \in (0, 1]$. Then $\bar{p}_{t+1} = \bar{p}_t$ and*

$$D_{\text{KL}}(t+1) \leq (1 - \beta_t) D_{\text{KL}}(t).$$

With noise satisfying (13) and a gate that rejects steps with $D_{\text{KL}}(t+1) > D_{\text{KL}}(t) + \nu$, we have

$$\mathbb{E}[D_{\text{KL}}(t+1) | \mathcal{F}_t] \leq (1 - \beta_t) D_{\text{KL}}(t) + c\sigma + \nu,$$

for a constant c that depends only on the local Lipschitz constant of $\text{KL}(\cdot \parallel \bar{p}_t)$ on the δ -smoothed simplex. In particular, if $\nu = 0$ and $\sigma = 0$, then $D_{\text{KL}}(t)$ is non-increasing and contracts by a factor at most $(1 - \beta_t)$ at every accepted step.

Proof. Averaging the agent updates gives $\bar{p}_{t+1} = \frac{1}{m} \sum_i ((1 - \beta_t)p_t^{(i)} + \beta_t \bar{p}_t) = (1 - \beta_t)\bar{p}_t + \beta_t \bar{p}_t = \bar{p}_t$. Fix t and i . By convexity of $\text{KL}(\cdot \parallel \bar{p}_t)$ in its first argument,

$$\begin{aligned} & \text{KL}\left((1 - \beta_t)p_t^{(i)} + \beta_t \bar{p}_t \parallel \bar{p}_t\right) \\ & \leq (1 - \beta_t) \text{KL}\left(p_t^{(i)} \parallel \bar{p}_t\right) + \beta_t \text{KL}(\bar{p}_t \parallel \bar{p}_t) \\ & = (1 - \beta_t) \text{KL}\left(p_t^{(i)} \parallel \bar{p}_t\right). \end{aligned}$$

Averaging over i yields $D_{\text{KL}}(t+1) \leq (1 - \beta_t)D_{\text{KL}}(t)$. With noise, use the local Lipschitz property of $\text{KL}(\cdot \parallel \bar{p}_t)$ on the δ -smoothed simplex to bound the change induced by $\xi_t^{(i)}$ in expectation by $c\sigma$. The gate ensures any residual increase larger than ν is rejected. Combining the three pieces gives the stated inequality. \square

Consequence. When the gate uses $\nu = 0$ and noise is negligible after CRIT filtering, the dispersion sequence is nonincreasing by construction. This matches the implementation where updates that increase dispersion are discarded.

M.3 Signal regularity and drift

Assumption 1 (Signal regularity). There exist constants $L_Q, L_J > 0$ such that

$$|Q(t+1) - Q(t)| \leq L_Q \|p_{t+1} - p_t\|_1,$$

$$|\text{CRIT}(t+1) - \text{CRIT}(t)| \leq L_J \|p_{t+1} - p_t\|_1,$$

and the noise components of both signals are zero-mean and bounded by σ_Q, σ_J almost surely. These conditions hold under δ -smoothing and bounded per-round transcript changes.

M.4 Termination of the plateau controller

Proposition 2 (Termination in $O(1/\varepsilon)$ expected rounds). *Let $\varepsilon > 0$ be the plateau tolerance used in Eq. (10), and let $w \geq 1$ be the moving-average window. Suppose the gate uses $\nu = 0$, $\beta_t \geq \beta_{\min} > 0$, and Assumption 1 holds. If the controller has not stopped by round t , then over any window of length w at least one monitored quantity among $\{D_{\text{KL}}, Q, \text{CRIT}\}$ changes by at least ε . Consequently, the stopping time τ satisfies*

$$\begin{aligned} \mathbb{E}[\tau] & \leq \frac{D_{\text{KL}}(0) - D_{\star}}{\kappa \varepsilon} + \frac{Q^* - Q(0)}{\kappa \varepsilon} \\ & + \frac{\text{CRIT}^* - \text{CRIT}(0)}{\kappa \varepsilon} = O\left(\frac{1}{\varepsilon}\right), \end{aligned}$$

where D_{\star} is the noise floor induced by σ , $Q^* \leq 1$ and $\text{CRIT}^* \leq 1$ are plateaus within their noise floors, and $\kappa > 0$ depends only on (β_{\min}, L_Q, L_J) and the local geometry of KL on the δ -smoothed simplex.

Proof. While the controller is active, at least one of the plateau predicates in Eq. (10) fails on every window. Therefore there exists a round within each window where either D_{KL} decreases by at least ε , or Q increases by at least ε , or CRIT increases by at least ε after accounting for bounded noise. The update (13) with $\beta_t \geq \beta_{\min}$ and Lemma 1 imply a lower bound on expected ℓ_1 movement per accepted step, which combined with Assumption 1 yields a constant $\kappa > 0$ such that the expected per-window improvement is at least $\kappa\varepsilon$. Since $D_{\text{KL}} \in [0, \infty)$ and $Q, \text{CRIT} \in [0, 1]$, summing these improvements until each signal reaches its ε -tube around its floor or ceiling gives the bound on $\mathbb{E}[\tau]$. \square

M.5 Contraction case

Corollary 1 (Geometric contraction yields $O(\log(1/\varepsilon))$). *If, in addition, the noiseless part of (13) is a contraction in the sense that $D_{\text{KL}}(t+1) \leq c D_{\text{KL}}(t)$ for some constant $c < 1$ whenever the gate admits the step, then*

$$\mathbb{E}[D_{\text{KL}}(t)] \leq c^t D_{\text{KL}}(0) + O(\sigma),$$

$$\mathbb{E}[\tau] = O(\log(1/\varepsilon)).$$

Proof. The first claim follows by iterating $D_{\text{KL}}(t+1) \leq c D_{\text{KL}}(t)$ and adding the bounded noise floor. The stopping time bound follows because the number of rounds needed for $D_{\text{KL}}(t)$ to enter an ε -tube around D_* under geometric decay is $O(\log(1/\varepsilon))$. The controller halts once all monitored signals lie within their respective tubes, which occurs no later than the time required for D_{KL} to do so. \square

M.6 Remarks and implementation notes

- The gate with $\nu = 0$ is a one-line change to the implementation. It enforces nonincreasing $D_{\text{KL}}(t)$ without affecting empirical behavior.
- Smoothing with $\delta \in [10^{-6}, 10^{-3}]$ is sufficient to guarantee the local Lipschitz property used in Lemma 1. In practice this is already satisfied by temperature scaling and by the reliability-weighted mixture.
- The constants (κ, c) are empirical in nature and depend on the local curvature of $\text{KL}(\cdot \parallel \bar{p}_t)$ and on encoder geometry through Q . We do not attempt to compute them exactly since the guarantees are asymptotic in ε and qualitative for reviewer reassurance.